ISSN 0280–5316
ISRN LUTFD2/TFRT--5714--SE

Side Wind Compensation using Active Suspension

Max Lindholm

Department of Automatic Control
Lund Institute of Technology
October 2003

Department of Automatic Control
Lund Institute of Technology
Box 118
SE-221 00 Lund Sweden

Document name
MASTER THESIS

Date of issue
October 2003

Document Number
ISRN LUTFD2/TFRT--5714--SE

Author(s)
Max Lindholm

Supervisor
Jens Kalkkuhl, DaimlerChrysler AG
Anders Rantzer,LTH

Sponsoring organization

Title and subtitle
Side Wind Compensation using Active Suspension (Sidvindskompensering m. h .a. aktiv fjädring)

Abstract
This thesis investigates what mechanisms that contribute to the interaction between lateral and vertical dynamics in a four-wheeled vehicle. For this a vehicle model was derived. To capture all the essential dynamics of the vehicle, both a horizontal model and a vertical model was used. The interaction between the models turned out to be quite evident, making it possible to use the active suspension system to influence the yaw dynamics of the vehicle. Further, it was investigated how this effect could be used for attenuating the effects of wind gusts. Since steer by wire is still a topic of active research and it´s integration into vehicles lies in the future, this cannot presently be used for side wind rejection. With the vehicle model, it was possible to design a feedback controller that uses the active suspension system for side wind rejection.

Keywords
Active suspension, side wind rejection, vehicle dynamics, PID control

Classification system and/or index terms (if any)

Supplementary bibliographical information

ISSN and key title
0280-5316

ISBN

Language
English

Number of pages
70

Recipient's notes

Security classification

Acknowledgment

This project was carried out at one of Daimler Chrysler AG's research departments (RIC/AR) in Esslingen, Germany from November 2002 to May 2003. I would like to thank all the people at the department that have helped me throughout my work, especially Prof. Jens Kalkkuhl and Dipl.-Ing. Magnus Rau for their support and supervising. I would also like to thank Prof. Anders Rantzer for giving me the opportunity and for his support.

Contents

1. Introduction

In today's development of automotive systems a major field of research is how to develop systems that assist the driver in certain driving situations, increasing the comfort and safety of the driver. Example of such systems are controllers for the vertical, longitudinal and lateral movements of the vehicle. ABS (Anti-lock Braking system) is already standard in most vehicles whereas ABC (Active Body Control) is taking a step from being a part of upmarket vehicles to become standard in more ordinary cars. Another system that has not yet been implemented into cars in most countries is the SBW system (Steer by Wire), where the mechanical components of the steering system will be replaced with electrical hardware. The SBW system is still a topic of active research.

1.1 Background

The automotive control systems have largely been designed independently of each other ignoring the coupling that exists between them, e.g. when controlling the horizontal dynamics, the vertical dynamics is affected and vice versa. Therefore more effort is put into the integration of these systems, to make overall vehicle optimization possible. One part of optimizing the vehicle dynamics, is to reduce the effects from disturbances such as wind gusts.

Lateral disturbances that are caused by heavy wind gusts can reduce the safety of the driver and the passengers, particulary if the driver tend to overcompensate. Weaker wind gusts reduce the comfort and it is therefore desirable to reduce the effects these disturbances have on a vehicle. In earlier work, it has been investigated how the effects from wind gusts can be attenuated with the steer by wire system. Since this system may not be implemented for several years, the automotive industry is looking for other solutions.

1.2 Objectives

One of the main objectives with this work has been to investigate how the vertical and lateral dynamics influence each other. This was done by developing a vehicle model that closely represents the dynamics of a vehicle, particulary in the aspect of coupling the vertical dynamics with the lateral dynamics. A second main objective has been to find out what mechanisms that makes it possible to influence the steering behaviour using active suspension. In addition, how great is the influence on the lateral dynamics and could it be used for side wind rejection. If so, a controller should be designed.

1.3 Methods

The project started with finding mathematical equations that represents different dynamical parts of a four-wheeled vehicle. This was needed for linearisation of the model, thus being able to perform plant analysis and control design. Particulary, the equations for horizontal and vertical dynamics were needed, since a coupling between the models should be done. The equations were found in literature. When these models had been coupled, simulations using Matlab/Simulink showed that the model was insufficient. By deriving the dynamics of the steering system and adding this to the model, the match with the non-linear simulation package CASCaDE was significantly improved. Relying on simulations in CASCaDE and tests

on the departments test vehicle, the mechanisms that contributes to the coupling were found. Finally, the controller was designed using Matlab/SISO toolbox.

1.4 Thesis Outline

In the following chapters it will be discussed how the active suspension system, to some extent, can be used to influence the steering behaviour of the vehicle. In the final chapter the design of a controller is presented which attenuates the effects of wind gusts.

Chapter 2 The Vehicle Model

For analysis of a plant, a powerful tool is to transform the plant from time domain to frequency domain. When transforming a model to frequency domain, it is necessary for the model to be linear. The vehicle model which can be linearised about certain points and used for analysis is presented in this chapter. The coupling of the lateral and vertical models is also described. Some theory about aerodynamics and how it influences the behaviour of the vehicle is also given. Finally a short description of the complex and highly non linear simulation package CASCaDE (Computer Aided Simulation of Car and Driver Environment) is presented.

Chapter 3 Validation

The vehicle model is evaluated by comparing simulation results to simulations in CASCaDE and to tests performed using the departments test vehicle, the so called Technoshuttle. It is also discussed, in which situations and for what manoeuvres the linearised model can be used for analysis and simulation.

Chapter 4 Analysis of wind gust rejection

Some different possibilities in rejecting side winds are presented but the focus is kept at the active suspension system and it's limitations. The different mechanisms that contributes to the possibility of influencing the lateral dynamics with active suspension are presented, as well as to what extent the different mechanisms contribute.

Chapter 5 Control Design

The existing ABC system is presented in this chapter. Some changes needs to be done in the ABC system when implementing the new controller and this will also be discussed here. Finally, the results of the PID controller, and what limitations exist are presented.

Appendix

Parts of Matlab Code will be included and also a derivation of how sensor signals can be reconstructed from center of gravity values using classical kinematics.

2. Vehicle Model

2.1 Modelling of Vehicle Dynamics

Vehicle dynamics is concerned with the movements of vehicles on a road surface. The behaviour is determined by the forces imposed on the vehicle from the tyres, gravity and aerodynamics. The vehicle and it's components behaviour are studied under certain conditions to understand the mechanisms involved during certain manoeuvres.

This chapter describes the modelling of the car dynamics. The modelling can be simplified into four major submodels that can be connected. The first model describes the dynamics behind the horizontal motions such as the longitudinal and lateral velocities. The second model describes the vertical dynamics of the car body and the wheels. The third model represents the tyre behavior and the fourth model regards the dynamics of the steering system. The connections between the models are also presented in this chapter.

In the case of horizontal dynamics, the vehicle is represented as one lumped mass located at the center of gravity. When analysing the vertical movements of the car the wheels and the body are modelled as separate lumped masses. Figure 2.1 shows the vehicles six degrees of freedom. The equations for the horizontal dynamics considers three degrees of freedom, the yaw as well as the longitudinal and lateral motions. In the vertical model, the other three degrees of freedom are considered, the roll, pitch and lift motions.

2.2 Horizontal dynamics of a four-wheel vehicle

The vehicle motion is described with reference to two different coordinate systems, one that is fixed to the body and one that is global[7]. The center of gravity is used as the origin for the body fixed coordinate system and it is following the motion of the vehicle.The earth fixed coordinate system has an arbitrarily defined origin. The current rotation of the body-fixed system in relation to the global coordinate system is described by the yaw angle Ψ. Disregarding Ψ, all quantities are defined

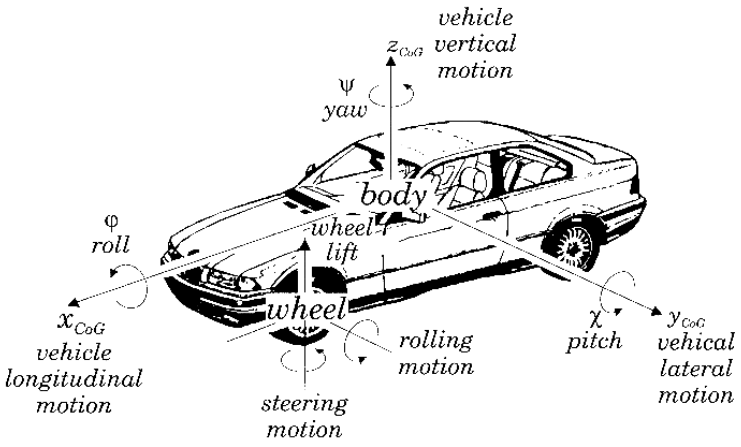

Figure 2.1 The vehicles six degrees of freedom.

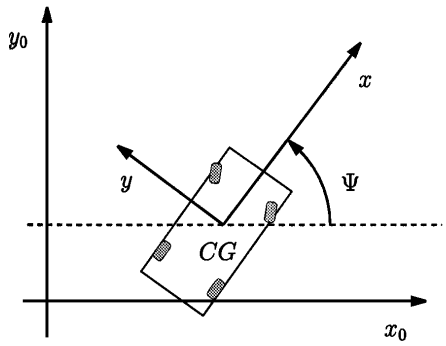

Figure 2.2 Definition of earth and body-fixed coordinate system.

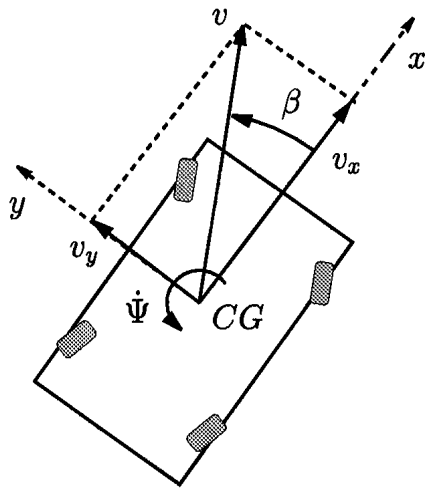

Figure 2.3 The center of gravity co-ordinate system and its main quantities.

in the body-fixed coordinate system. However, only the time derivative of the of the yaw angle $\dot{\Psi}$ is of interest here. Thus, the orientation of the body-fixed system in the global system is not relevant.

The x-axis points forward in the longitudinal direction of the vehicle, the y-axis in the lateral direction and the z-direction is defined positive in upward direction. The horizontal motion of the vehicle can be described by three quantities $(v_x, v_y, \dot{\psi})$, and these are illustrated in Figure 2.3. Explanations of the symbols can be found in table 2.1.

Figure 2.4 shows the body-fixed coordinate system and the four corners represent the respective tyre footprints [1]. For given γ_i and h_i $(i = 1, ..., 4)$, the geometric system is defined by

$$b_i = h_i \sin \gamma_i \tag{2.1}$$

$$l_i = h_i \cos \gamma_i \tag{2.2}$$

To simplify notations a generalized quarter-car (see Figure 2.5) is used. The geometric quantities in this figure relate to those in Figure 2.4 via the geometry equations in table 2.2.

[1]The contact between a pneumatic tyre and the ground is actually not a point but rather a patch. In the model derived here, the contact patch is considered as a point, about which all forces are acting.

Table 2.1 Coordinate system variables for the horizontal model

v_x	The forward velocity, in the direction of x_{CG}
v_y	The lateral velocity, in the direction of y_{CG}
$\dot{\psi}$	Yaw rate (rotation about z_{CG})
δ_i	Wheel steering angle
v	The resulting velocity
β	Vehicle body side slip angle (angle between x_{CG} and v_{CG}, the vehicle velocity)
F_{yi}	Lateral wheel ground contact force (acting in the direction of y_{Wi})
F_{xi}	Longitudinal wheel ground contact force (acting in the direction of x_{Wi})

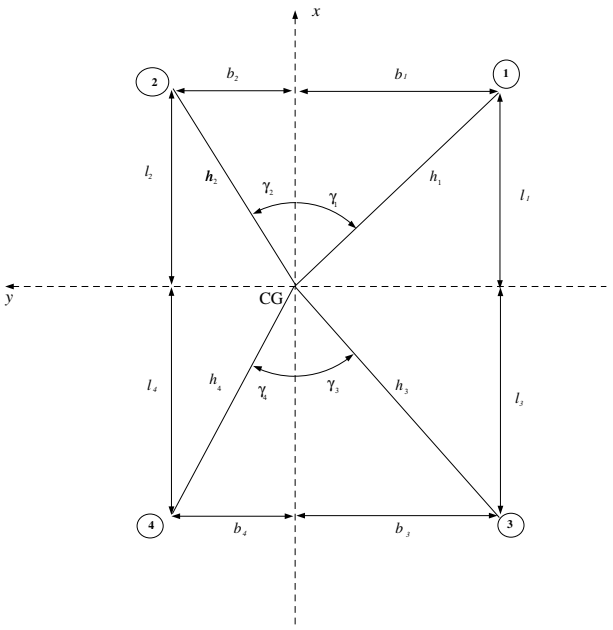

Figure 2.4 Vehicle axis system and geometric definitions

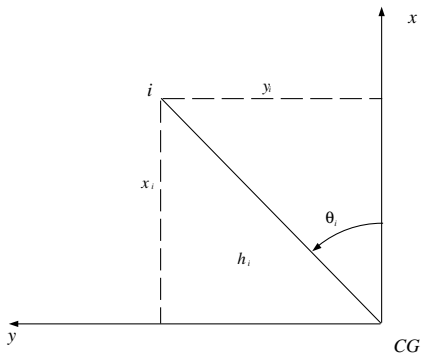

Figure 2.5 Vehicle axis system and geometric definitions

Table 2.2 Relationship between quarter-car, Figure 2.5 and the complete model Figure 2.4

$\theta_1 = -\gamma_1$	$x_1 = l_1$	$y_1 = -b_1$
$\theta_2 = \gamma_2$	$x_2 = l_2$	$y_2 = b_2$
$\theta_3 = \pi + \gamma_3$	$x_3 = -l_3$	$y_3 = -b_3$
$\theta_4 = \pi - \gamma_4$	$x_4 = -l_4$	$y_4 = b_4$

Equations of motions for the horizontal model

The force components f_{xi} and f_{yi} indicate the components of the forces generated by the tyres in body-fixed coordinates (see Figure 2.6):

$$f_{xi} = F_{xi}\cos\delta_i - F_{yi}\sin\delta_i \tag{2.3}$$
$$f_{yi} = F_{xi}\sin\delta_i + F_{yi}\cos\delta_i \tag{2.4}$$

By using Newton's second law ($\sum \boldsymbol{F} = m\boldsymbol{a}$), the resulting equations of motions are:

$$ma_x = \sum_{i=1}^{4}(F_{xi}\cos\delta_i - F_{yi}\sin\delta_i) \tag{2.5}$$

$$ma_y = \sum_{i=1}^{4}(F_{xi}\sin\delta_i + F_{yi}\cos\delta_i) \tag{2.6}$$

where $a_x = \dot{v}_x - v_y\dot{\psi}$ and $a_y = \dot{v}_y + v_x\dot{\psi}$.

The torque caused by the forces at a single wheel, m_i, and acting on the center of gravity are:

$$m_i = h_i(-f_{xi}\sin\theta_i + f_{yi}\cos\theta_i) \tag{2.7}$$

The balance of torques for plane motion (around z-axis) is described by $\sum M_z = I_{zz}\ddot{\psi} = \sum m_i$ and we get

$$I_{zz}\ddot{\psi} = \sum_{i=1}^{4} h_i(-f_{xi}\sin\theta_i + f_{yi}\cos\theta_i) \tag{2.8}$$

Equation 2.5-2.8 are the equations describing the horizontal dynamics assuming that the forces on the tyres are known.

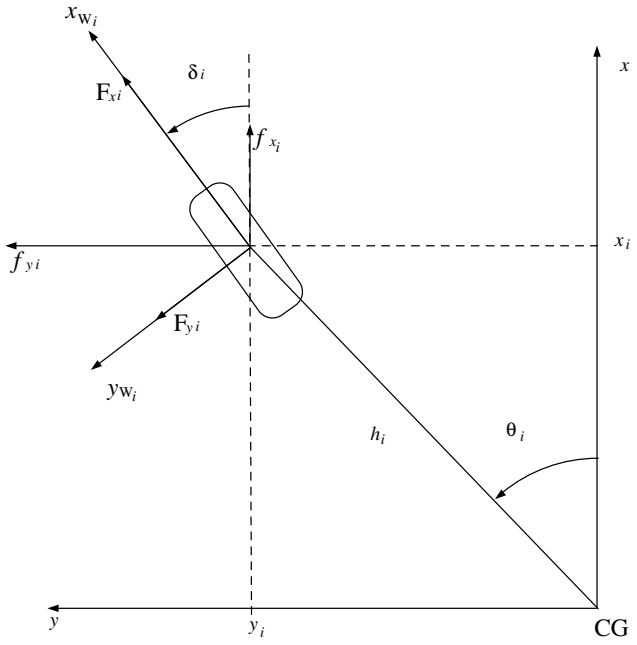

Figure 2.6 Definition of tyre forces and steer angle

2.3 Vertical dynamics of a four-wheel vehicle

In Figure 2.7 the geometry of the vehicle model is described. The body of the car is modelled as a stiff body with three degrees of freedom (according to [6]). The motions of the body is described by the vertical motion z_B, the roll angle r (rotational motion about the $x-axis$), and the pitch angle p (rotational motion about the $y-axis$). The axles are modelled as weightless bars. The actuators are acting on the springs of the suspension system and these are assumed to be linear. On a suspension strut, a linear damper is assumed to be mounted parallel to the spring and actuator.

The wheels are modelled as point masses with linear spring characteristics. According to [6], the damping of the wheels are small enough to be neglected. The wheels are assumed to move only in the vertical direction and the motion of the wheel is described by the wheel position, z_W.

Further, the axles are modelled as if they were parallel, and by doing so, the relative longitudinal and lateral motions between the axles and the body are not considered. The outside forces and moments that arises during acceleration, braking, cornering etc are M_r, M_p and F_z as described in Figure 2.7.

Equations of motions for the vertical model

The conditions for the linearisation of the model is that the roll and pitch angles remains small, that all forces act perpendicular to the body and that the vertical movement of the body is small.

If considering $F_{B\_i} = F_{ss\_ii}$ and $l_{B\_i} = l_{ss\_i}$, Newton's second law (see Figure 2.8) for the vertical motion becomes:

$$m_B\ddot{z}_B = F_{ss\_fr} + F_{ss\_fl} + F_{ss\_rr} + F_{ss\_rl} - F_{L\_fr} - F_{L\_fl} - F_{L\_rr} - F_{L\_rl} + F_z \quad (2.9)$$

The balance of torques equation (about x- and y-axis respectively) gives us:

$$\begin{aligned} J_p\ddot{p} = &-l_f\cos(p)(F_{ss\_fr} + F_{ss\_fl}) + l_{r^*}\cos(p)(F_{ss\_rr} + F_{ss\_rl}) + \\ &+ l_f\cos(p)(F_{L\_fr} + F_{L\_fl}) - l_{r^*}\cos(p)(F_{L\_rr} + F_{L\_rl}) + M_p \end{aligned} \quad (2.10)$$

$$\begin{aligned} J_r\ddot{r} = &(F_{ss\_fl}l_{ss\_fl} + F_{ss\_rl}l_{ss\_rl})\cos(r) - (F_{ss\_fr}l_{ss\_fr} + F_{ss\_rr}l_{ss\_rr})\cdot \\ &\cdot\cos(r) - (F_{L\_fl}l_{L\_fl} + F_{L\_rl}l_{L\_rl})\cos(r) + (F_{L\_fr}l_{L\_fr} + F_{L\_rr}l_{L\_rr})\cdot \\ &\cdot\cos(r) + M_r \end{aligned} \quad (2.11)$$

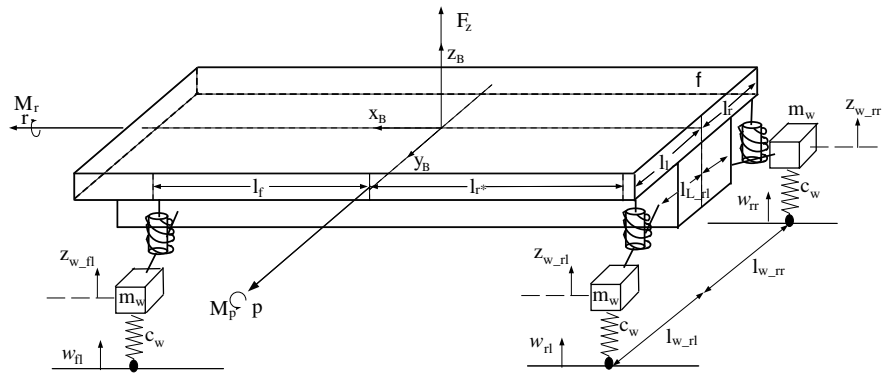

Figure 2.7 Linear vertical vehicle model

Table 2.3 Parameters and variables of linear vertical model

x_B, y_B, z_B	Axis for the center of gravity co-ordinate system
l_f, l_{r^*}	The x-component of the distance from CG to suspension systems front and rear
l_l, l_r	The y-component of the distance from CG to suspension system
l_{L_i}	The y-component of the distance from CG to bearing mount
l_{W_i}	The y-component of the distance from CG to wheel
l_{ss_i}	The y-component of the distance from CG to suspension strut
$l_{fr}, l_{fl}, l_{rr}, l_{rl}$	The indices stands for Front Right .. Rear Left
z_{PP}, z_{RP}	The vertical distance from ground level to the pitch- and roll axis respectively
z_{B0}	The vertical distance from ground level to CG
z_L	The vertical distance from ground level to bearing mount
z_{ssB}	The vertical distance from ground level to upper suspension mounting point
z_{ssL}	The vertical distance from ground level to lower suspension mounting point
r, p	Roll- and pitch angle respectively
M_r, M_p	Roll- and pitch moment respectively
J_x, J_y	Roll- and pitch moment of inertia respectively
F_z	Disturbance force in vertical direction
m_B, m_W	Body- and wheel mass respectively
$\underline{F}_{ss}$	Forces in suspension strut
$\underline{F}_L$	Forces in bearing mount
c_{Bf}, c_{Br}	Suspension spring constants front and rear
b_{Bf}, b_{Br}	Suspension damper constants front and rear
u_{ij}	Suspension system control signal
c_W	Tyre spring constant
w_{ij}	Road profile at tyre contact "point"

Moments of inertia about roll and pitch axis are calculated according to Steiner's theorem. It is assumed that the roll and pitch axes are parallel to the x and y axes respectively.

$$J_r = J_x + m_B(z_{B0} - z_{RP})^2 \tag{2.12}$$

$$J_p = J_y + m_B(z_{B0} - z_{PP})^2 \tag{2.13}$$

Linearising eq 2.9-eq 2.11 and introducing the matrices:

$$\Theta_B = \begin{pmatrix} m_B & 0 & 0 \\ 0 & J_p & 0 \\ 0 & 0 & J_r \end{pmatrix} \tag{2.14}$$

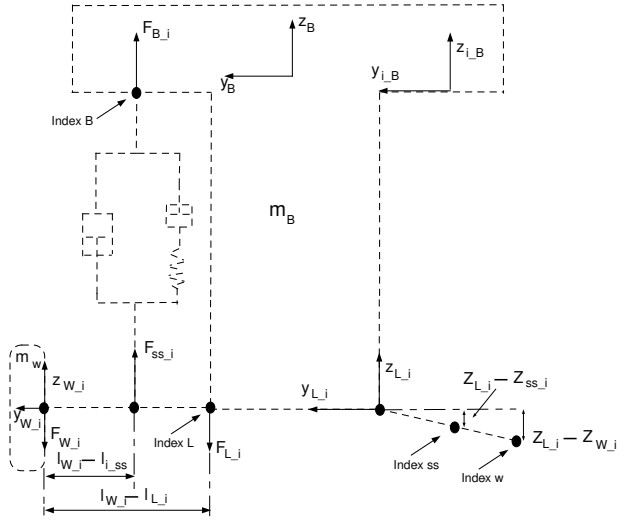

Figure 2.8 Forces acting upon body, wheels and suspension system

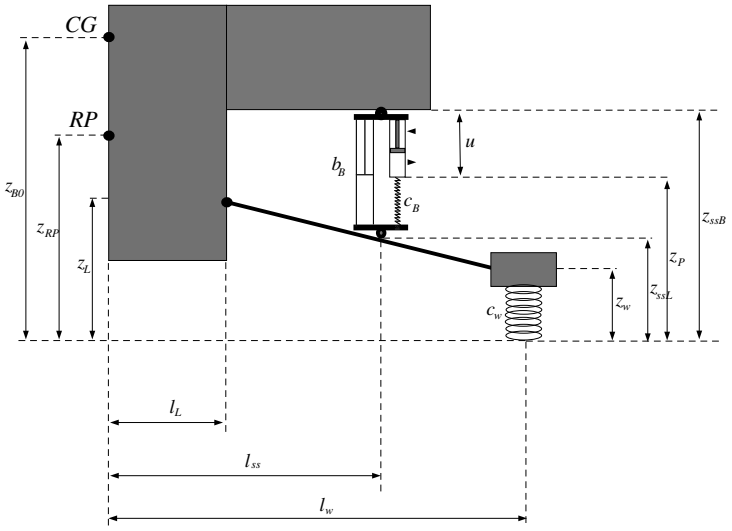

Figure 2.9 Geometry of axle and suspension system

,

$$\underline{F}_B = \underline{F}_{ss} = \begin{pmatrix} F_{ss\_fr} \\ F_{ss\_fl} \\ F_{ss\_rr} \\ F_{ss\_rl} \end{pmatrix} \text{ and } \underline{F}_L = \begin{pmatrix} F_{L\_fr} \\ F_{L\_fl} \\ F_{L\_rr} \\ F_{L\_rl} \end{pmatrix} \tag{2.15}$$

we get

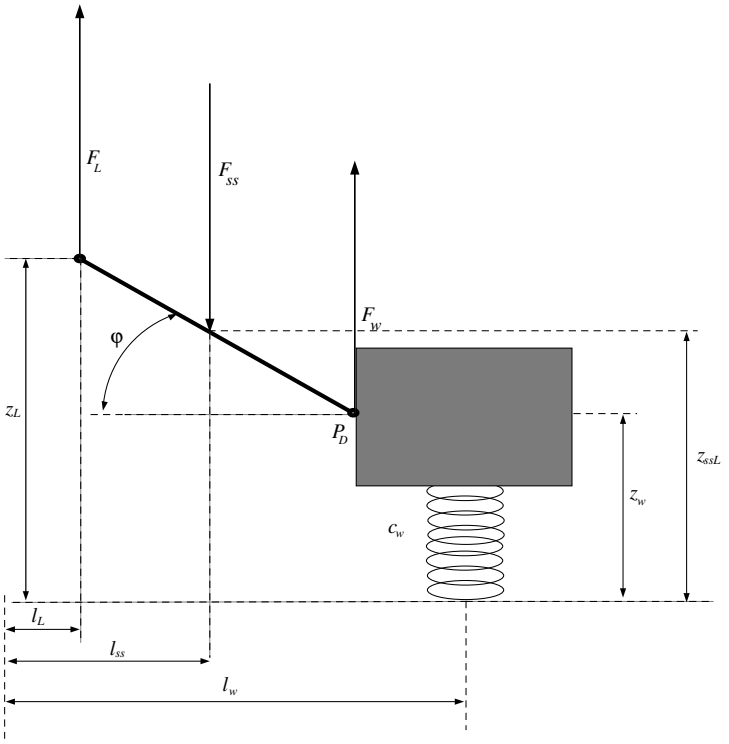

Figure 2.10 Bearing force determination by moment equilibrium around the point P_D

$$\Theta_B \begin{pmatrix} \ddot{z}_B \\ \ddot{p} \\ \ddot{r} \end{pmatrix} = \begin{pmatrix} 1 & 1 & 1 & 1 \\ -l_f & -l_f & l_{r^*} & l_{r^*} \\ -l_{ss\_fr} & l_{ss\_fl} & -l_{ss\_rr} & l_{ss\_rl} \end{pmatrix} \cdot \cdot \underline{F}_{ss} - \begin{pmatrix} 1 & 1 & 1 & 1 \\ -l_f & -l_f & l_{r^*} & l_{r^*} \\ -l_{L\_fr} & l_{L\_fl} & -l_{L\_rr} & l_{L\_rl} \end{pmatrix} \underline{F}_L + \begin{pmatrix} F_z \\ M_p \\ M_r \end{pmatrix} \tag{2.16}$$

By defining the geometry Matrices as

$$T_{G\_B} = T_{G\_ss} = \begin{pmatrix} 1 & -l_f & -l_{ss\_fr} \\ 1 & -l_f & l_{ss\_fl} \\ 1 & l_{r^*} & -l_{ss\_rr} \\ 1 & l_{r^*} & l_{ss\_rl} \end{pmatrix} \text{ and } T_{G\_L} = \begin{pmatrix} 1 & -l_f & -l_{L\_fr} \\ 1 & -l_f & l_{L\_fl} \\ 1 & l_{r^*} & -l_{L\_rr} \\ 1 & l_{r^*} & l_{L\_rl} \end{pmatrix} \tag{2.17}$$

we arrive at the more compact equation

$$\Theta_B \begin{pmatrix} \ddot{z}_B \\ \ddot{p} \\ \ddot{r} \end{pmatrix} = T_{G\_ss}^T \underline{F}_{ss} - T_{G\_L}^T \underline{F}_L + \begin{pmatrix} F_z \\ M_p \\ M_r \end{pmatrix} \tag{2.18}$$

If an equation of moment equilibrium is taken around the pivoted point P_D in Figure 2.10, the following relationship can be derived:

$$\underline{0} = (L_W - L_{ss})\underline{F}_{ss} - (L_W - L_L)\underline{F}_L \tag{2.19}$$

with the matrices

$$L_W = diag\left[\begin{pmatrix} l_{W\_fr} \\ l_{W\_fl} \\ l_{W\_rr} \\ l_{W\_rl} \end{pmatrix}\right], \; L_L = diag\left[\begin{pmatrix} l_{L\_fr} \\ l_{L\_fl} \\ l_{L\_rr} \\ l_{L\_rl} \end{pmatrix}\right]$$

$$\text{and } L_{ss} = diag\left[\begin{pmatrix} l_{ss\_fr} \\ l_{ss\_fl} \\ l_{ss\_rr} \\ l_{ss\_rl} \end{pmatrix}\right]. \quad (2.20)$$

we arrive at

$$\underline{F}_L = (L_W - L_L)^{-1}(L_W - L_{ss})\underline{F}_{ss} \quad (2.21)$$

A simpler form of equation 2.21 occurs if $(L_W - L_L)^{-1}(L_W - L_{ss})$ is rewritten to:

$$\begin{aligned}(L_W - L_L)^{-1}(L_W - L_{ss}) &= (L_W - L_L)^{-1}(L_W - L_{ss} + L_L - L_L) = \\ &= \underbrace{(L_W - L_L)^{-1}(L_W - L_L)}_{=I_4} - \underbrace{(L_W - L_L)^{-1}(L_W - L_{ss})}_{:=H}\end{aligned} \quad (2.22)$$

Now, the bearing force can be calculated directly from the suspension force through $\underline{F}_L = (I_4 - H)\underline{F}_{ss}$.

Equation 2.18 can now be simplified to

$$\Theta_B \begin{pmatrix} \ddot{z}_B \\ \ddot{p} \\ \ddot{r} \end{pmatrix} = \left(T^T_{G\_ss} - T^T_{G\_L}(I_4 - H)\right)\underline{F}_{ss} + \begin{pmatrix} F_z \\ M_p \\ M_r \end{pmatrix} \quad (2.23)$$

and with the definition $T^{*T}_G = T^T_{G\_ss} - T^T_{G\_L}(I_4 - H)$ it is further reduced to

$$\Theta_B \begin{pmatrix} \ddot{z}_B \\ \ddot{p} \\ \ddot{r} \end{pmatrix} = T^{*T}_G \underline{F}_{ss} + \begin{pmatrix} F_z \\ M_p \\ M_r \end{pmatrix} \quad (2.24)$$

.

The suspension forces that acts on the body are determined from the suspension system properties. They are dependent on the spring and damper characteristics as well as on the control signal from the control system actuator (see Figure 2.9).

The suspension system spring and damper matrices are defined in equation 2.25

$$A_1 = \begin{pmatrix} c_{Bf} & 0 & 0 & 0 \\ 0 & c_{Bf} & 0 & 0 \\ 0 & 0 & c_{Br} & 0 \\ 0 & 0 & 0 & c_{Br} \end{pmatrix} \text{ and } A_2 = \begin{pmatrix} b_{Bf} & 0 & 0 & 0 \\ 0 & b_{Bf} & 0 & 0 \\ 0 & 0 & b_{Br} & 0 \\ 0 & 0 & 0 & b_{Br} \end{pmatrix} \quad (2.25)$$

The forces can be expressed as:

$$\underline{F}_{ss} = A_1(\underline{z}_{ssL} - \underline{z}_P) + A_2(\dot{\underline{z}}_{ssL} - \dot{\underline{z}}_{ssB}) \quad (2.26)$$

By using the theorem on intersecting lines in Figure 2.9, the following geometrical relationship can be derived.

$$\frac{z_L - z_w}{l_L - l_w} = \frac{z_L - z_{ssL}}{l_L - l_{ss}} \tag{2.27}$$

Writing equation 2.27 into vectorial form we get:

$$(L_L - L_{ss})(\underline{z}_L - \underline{z}_w) = (L_L - L_w)(\underline{z}_L - \underline{z}_{ssL}) \tag{2.28}$$

Solving for $\underline{z}_{ssL}$ and using the previously defined matrix H, results in:

$$\begin{aligned} \underline{z}_{ssL} &= \underline{z}_L - (L_L - L_w)^{-1}(L_L - L_{ss})(\underline{z}_L - \underline{z}_w) = \underline{z}_L - H(\underline{z}_L - \underline{z}_w) = \\ &= (I_4 - H)\underline{z}_L + H\underline{z}_w \end{aligned} \tag{2.29}$$

The vertical distance from ground level to bearing mount, $\underline{z}_L$ can be expressed in the three coordinates associated with the body as in equation 2.30.

$$\underline{z}_L = T_{G\_L} \begin{pmatrix} z_B \\ p \\ r \end{pmatrix} \tag{2.30}$$

By inserting equation 2.30 into equation 2.29, the result is:

$$\underline{z}_{ssL} = (I_4 - H)T_{G\_L} \begin{pmatrix} z_B \\ p \\ r \end{pmatrix} + H\underline{z}_w \tag{2.31}$$

and equation 2.26 can be written as

$$\begin{aligned} \underline{F}_{ss} = A_1 &\left((I_4 - H)T_{G\_L} \begin{pmatrix} z_B \\ p \\ r \end{pmatrix} + H\underline{z}_w - \underline{z}_P \right) + \\ &+ A_2 \left((I_4 - H)T_{G\_L} \begin{pmatrix} \dot{z}_B \\ \dot{p} \\ \dot{r} \end{pmatrix} + H\dot{\underline{z}}_w - \dot{\underline{z}}_{ssB} \right) \end{aligned} \tag{2.32}$$

If one considers

$$\underline{z}_{ssB} = T_{G\_ss} \begin{pmatrix} z_B \\ p \\ r \end{pmatrix} \tag{2.33}$$

and the geometric relation $\underline{u} = \underline{z}_{ssB} - \underline{z}_P$, the equation for the forces in the suspension struts can be written as:

$$\begin{aligned} \underline{F}_{ss} = A_1 &\left(\left((I_4 - H)T_{G\_L} - T_{G\_ss} \right) \begin{pmatrix} z_B \\ p \\ r \end{pmatrix} + H\underline{z}_w + \underline{u} \right) + \\ &+ A_2 \left(\left((I_4 - H)T_{G\_L} - T_{G\_ss} \right) \begin{pmatrix} \dot{z}_B \\ \dot{p} \\ \dot{r} \end{pmatrix} + H\dot{\underline{z}}_w \right) \end{aligned} \tag{2.34}$$

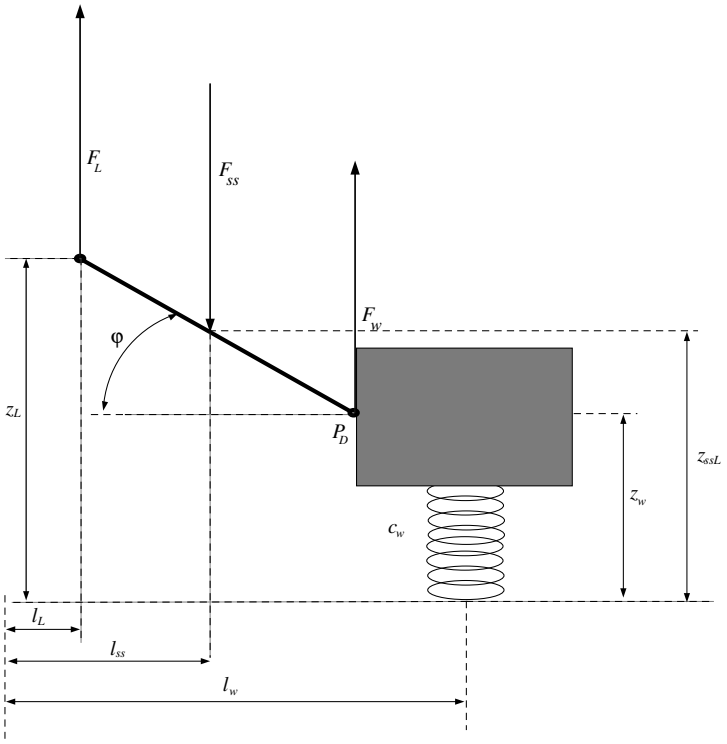

Figure 2.11 Bearing force determination by moment equilibrium around the point P_D

If one considers the previously defined:

$$T_G^{*T} = T_{G\_ss}^T - T_{G\_L}^T(I_4 - H) = T_{G\_ss} - (I_4 - H)T_{G\_L}{}^2 \tag{2.35}$$

and inserts this into equation 2.34 a simpler form arises:

$$\underline{F}_{ss} = A_1 H \underline{z}_w + A_2 H \dot{\underline{z}}_w + A_1 \underline{u} - A_1 T_G^* \begin{pmatrix} z_B \\ p \\ r \end{pmatrix} - A_2 T_G^* \begin{pmatrix} \dot{z}_B \\ \dot{p} \\ \dot{r} \end{pmatrix} \tag{2.36}$$

The attained equations for the forces in the suspension struts, is the inserted into the body's differential equations, i.e. equation 2.24.

$$\begin{aligned} &\Theta_B \begin{pmatrix} \ddot{z}_B \\ \ddot{p} \\ \ddot{r} \end{pmatrix} + T_G^{*T} A_2 T_G^* \begin{pmatrix} \dot{z}_B \\ \dot{p} \\ \dot{r} \end{pmatrix} + T_G^{*T} A_1 T_G^* \begin{pmatrix} z_B \\ p \\ r \end{pmatrix} \\ &= T_G^{*T} A_1 H \underline{z}_w + T_G^{*T} A_2 H \dot{\underline{z}}_w + T_G^{*T} A_1 \underline{u} + \begin{pmatrix} F_z \\ M_p \\ M_r \end{pmatrix} \end{aligned} \tag{2.37}$$

To determine the equations of motion for the wheels, a force equilibrium from Figure 2.11 is needed. The following equation describes the force equilibrium,

$$\underline{F}_w = \underline{F}_{ss} - \underline{F}_L = \underline{F}_{ss} - (I_4 - H)\underline{F}_{ss} = H\underline{F}_{ss} \tag{2.38}$$

[2] $(I_4 - H) = (I_4 - H)^T$ since it's a diagonal matrix

and the vertical dynamics of the wheel is be described as

$$m_W \ddot{\underline{z}}_w = -c_W(\underline{z}_w - \underline{w}) - \underline{F}_w = -c_W(\underline{z}_w - \underline{w}) - H\underline{F}_{ss} \tag{2.39}$$

By inserting equation 2.36 into equation 2.39 we get:

$$\begin{aligned} m_W \ddot{\underline{z}}_w = -c_W(\underline{z}_w - \underline{w}) - H\Bigg(& A_1 H \underline{z}_w + A_2 H \dot{\underline{z}}_w + A_1 \underline{u} - \\ & - A_1 T_G^* \begin{pmatrix} z_B \\ p \\ r \end{pmatrix} - A_2 T_G^* \begin{pmatrix} \dot{z}_B \\ \dot{p} \\ \dot{r} \end{pmatrix} \Bigg) \end{aligned} \tag{2.40}$$

Equation 2.40 and equation 2.37 is now represented together as one state space system, equation 2.41,

$$\begin{pmatrix} \dot{z}_B \\ \dot{p} \\ \dot{r} \\ \dot{\underline{z}}_W \\ \ddot{z}_B \\ \ddot{p} \\ \ddot{r} \\ \ddot{\underline{z}}_W \end{pmatrix} = \begin{pmatrix} 0_{3x4} \\ 0_{4x4} \\ 0_{3x4} \\ I_4 \frac{c_W}{m_W} \end{pmatrix} \underline{w} + \begin{pmatrix} 0_{3x3} \\ 0_{4x3} \\ \Theta_B^{-1} \\ 0_{4x3} \end{pmatrix} \begin{pmatrix} F_z \\ M_p \\ M_r \end{pmatrix} +$$

$$\begin{pmatrix} 0_{3x3} & 0_{3x4} & I_3 & \dots \\ 0_{4x3} & 0_{4x4} & 0_{4x3} & \dots \\ -\Theta_B^{-1} T_G^{*T} A_1 T_G^* & \Theta_B^{-1} T_G^{*T} A_1 H & -\Theta_B^{-1} T_G^{*T} A_2 T_G^* & \dots \\ \frac{1}{m_W} H A_1 T_G^* & -\frac{1}{m_W}(c_W I_4 + H A_1 H) & \frac{1}{m_W} H A_2 T_G^* & \dots \end{pmatrix}$$

$$\begin{pmatrix} \dots & 0_{3x4} \\ \dots & I_4 \\ \dots & \Theta_B^{-1} T_G^{*T} A_2 H \\ \dots & -\frac{1}{m_W} H A_2 H \end{pmatrix} \cdot \begin{pmatrix} z_B \\ p \\ r \\ \underline{z}_W \\ \dot{z}_B \\ \dot{p} \\ \dot{r} \\ \dot{\underline{z}}_W \end{pmatrix} + \begin{pmatrix} 0_{3x4} \\ 0_{4x4} \\ \Theta_B^{-1} T_G^T A_1 \\ -\frac{1}{m_W} H A_1 \end{pmatrix} \underline{u} \tag{2.41}$$

To rewrite 2.41 into the form,

$$\dot{\underline{x}} = A\underline{x} + B\underline{u}^* \tag{2.42}$$

, the following sub-matrices are defined:

$$A_{sub} = \begin{pmatrix} -\Theta_B^{-1} T_G^{*T} A_1 T_G^* & \Theta_B^{-1} T_G^{*T} A_1 H & \dots \\ \frac{1}{m_W} H A_1 T_G^* & -\frac{1}{m_W}(c_W I_4 + H A H_1) & \dots \\ \dots & -\Theta_B^{-1} T_G^{*T} A_2 T_G^* & \Theta_B^{-1} T_G^{*T} A_2 H \\ \dots & \frac{1}{m_W} H A_2 T_G^* & -\frac{1}{m_W} H A_2 H \end{pmatrix} \tag{2.43}$$

$$B_{sub} = \begin{pmatrix} \Theta_B^{-1} T_G^{*T} A_1 \\ -\frac{1}{m_W} H A_1 \end{pmatrix} \tag{2.44}$$

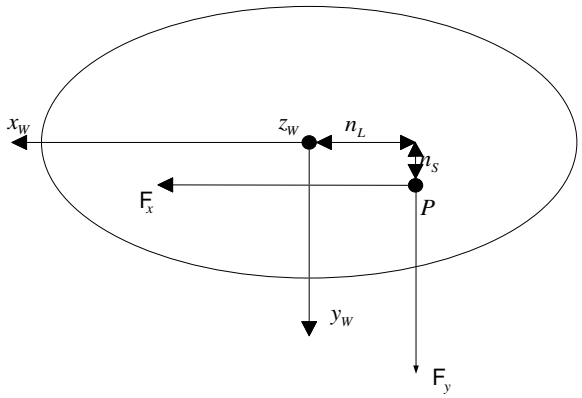

Figure 2.12 The wheel coordinate system viewed from above.

$$E_{sub} = \begin{pmatrix} \Theta_B^{-1} & 0_{3x4} \\ 0_{4x3} & I_4 \frac{c_W}{m_W} \end{pmatrix} \tag{2.45}$$

$$\underline{x} = \begin{pmatrix} z_B & p & r & \underline{z}_W & \dot{z}_B & \dot{p} & \dot{r} & \underline{\dot{z}}_W \end{pmatrix}^T \tag{2.46}$$

$$\underline{u}^* = \begin{pmatrix} \underline{u} & F_z & M_p & M_r & \underline{w} \end{pmatrix}^T \tag{2.47}$$

By using these notations, 2.41 is written as:

$$\underline{\dot{x}} = \begin{pmatrix} 0_{7x7} & I_{7x7} \\ A_{sub} & \end{pmatrix} \underline{x} + \begin{pmatrix} 0_{7x11} & \\ B_{sub} & E_{sub} \end{pmatrix} \underline{u}^* \tag{2.48}$$

2.4 Tyre Model

An important part of the modelling process is to have a good model of the forces acting on the tyres, since these have the biggest influence on the behaviour of the vehicle. The tyres are said to serve three basic functions. They should support vertical load while cushioning against road rocks, develop longitudinal forces for acceleration and braking and finally they should develop lateral forces while cornering. The forces that a tyre can develop are dependent on many different parameters. Vertical load, longitudinal and lateral stiffness and maximum friction are considered in the model used in this work. Other parameters such as tyre pressure, camber angle and temperature are not considered in the model[3].

The coordinate system of the tyre is defined in the same way as that of the vehicle, i.e. the x-axis points in the longitudinal direction of the wheel and the y-axis in the lateral. The location of the wheel ground contact point (marked by P in Figure 2.12) does not lie in the center of the wheels but due to caster towards the rear. Caster is the tilting of the steering axis either forward or backward (positive caster) from the vertical wheel axis. Positive caster provides stability to the vehicle, since it creates a self aligning torque around the vertical wheel axis. The wheel caster is a measure of the shift of the pressure distribution in the tyre

[3]An example of a more sophisticated tyre model, where more properties are considered can be found in [2].

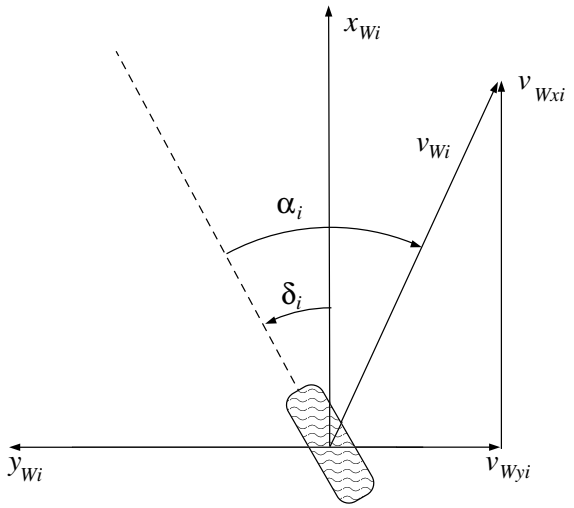

Figure 2.13 Tyre side slip angle in wheel coordinate system.

contact area. The forces (F_x and F_y in Figure 2.12) that are acting on the tyre at the contact point determine the dynamics of the vehicle. The characteristics of these forces are nonlinear with respect to the wheel slip, which is defined as

$$\lambda_{xi} = \frac{\omega_{Wi} r_{Wi} - v_{Wxi}}{v_W i} \tag{2.49}$$

$$\lambda_{yi} = \sin \alpha_i \tag{2.50}$$

$$\lambda_{Wi} = \sqrt{\lambda_{xi}^2 + \lambda_{yi}^2} \tag{2.51}$$

where ω_{Wi} is the angular velocity if the wheel, r_{Wi} is the dynamical radius of the wheel and v_{Wi} is defined as:

$$v_{Wxi} = v_x - \dot{\psi} h_i \sin \theta_i \tag{2.52}$$

$$v_{Wyi} = v_y + \dot{\psi} h_i \cos \theta_i \tag{2.53}$$

$$v_{Wi} = \sqrt{v_{Wxi}^2 + v_{Wyi}^2} \tag{2.54}$$

where v_{Wxi} is the longitudinal velocity of the wheel and v_{Wyi} the lateral velocity of the wheel.

The wheel slip is defined in the x- and y-directions of the wheel and a presence of the slip in y-direction λ_y causes the velocity vector of the wheel to have a direction different from x_W. The resulting angle (see Figure 2.13) is called *tyre side slip angle* and is defined as

$$\alpha_i = \delta_i + \arctan\left(\frac{-v_y - \dot{\psi} h_i \cos \theta_i}{v_x - \dot{\psi} h_i \sin \theta_i}\right) \tag{2.55}$$

The nonlinear model for stationary Lateral force F_y and stationary Longitudi-

nal force F_x is[4] (see [8])

$$F_y = \begin{cases} \frac{C_y \lambda_y}{(\xi_y - 1)^2 + C_y^* \xi_y} & \xi_y \leq 1, \\ \frac{\lambda_y}{\lambda_W} \mu_y F_z & \xi_y > 1 \end{cases} \tag{2.56}$$

$$F_x = \begin{cases} \frac{C_x \lambda_x}{(\xi_x - 1)^2 + C_x^* \xi_x} & \xi_x \leq 1, \\ \frac{\lambda_x}{\lambda_W} \mu_x F_z & \xi_x > 1 \end{cases} \tag{2.57}$$

with the following definitions of the normalised wheel slip

$$\xi_y = \frac{\lambda_W}{\lambda_{F_y max}} \qquad \xi_x = \frac{\lambda_W}{\lambda_{F_x max}} \tag{2.58}$$

and normalised stiffness

$$C_y^* = \frac{\lambda_{F_y max} C_y}{\mu_y F_z} \qquad C_x^* = \frac{\lambda_{F_x max} C_x}{\mu_x F_z} \tag{2.59}$$

μ_x and μ_y are the friction coefficients in longitudinal and lateral direction respectively,

$$\mu_x = \left(M_{x0} - M_{x1} \frac{F_Z}{F_{ZN}} \right) \mu_H \qquad \mu_y = \left(M_{y0} - M_{y1} \frac{F_Z}{F_{ZN}} \right) \mu_H \tag{2.60}$$

, where μ_H is the friction coefficient between the road and the tyre. F_Z is the wheel load, whereas F_{ZN} is the normalising wheel load. The parameters $M_{x0} \dots M_{y1}$ are parameters identified to fit measurement data.

C_x and C_y are the stiffness of the tyre in longitudinal and lateral direction respectively, whereas C_{x0} and C_{y0} are parameters identified to fit measurements.

$$C_x = C_{x0} \frac{F_Z}{F_{ZN}} \qquad C_y = C_{y0} \sin\left(2 \arctan\left(\frac{F_Z}{F_{ZN}} \right) \right) \tag{2.61}$$

$$\lambda_{F_x max} = L_{x0} \mu_H \qquad \lambda_{F_y max} = \sin\left(L_{y0} + L_{y1} \frac{F_Z}{F_Z N} \right) \mu_H \tag{2.62}$$

The equations describing the forces of the tyre are only valid in steady state, i.e. when the time derivatives of the wheel slip, $\dot{\lambda}_x = \dot{\lambda}_y = 0$. If fast changes in the slip needs to be considered, the dynamics of the tyre forces have to be included into the model [8].

In this work, only the model for the dynamic lateral force $\dot{F}_y$ is considered (eq 2.63).

$$\dot{F}_y = a \cdot \left(\overline{F}_y(\alpha) - F_y \right) = \frac{v_{Wx}}{0.03 v_{Wx} + 0.5} \left(C_y \alpha - F_y \right) \tag{2.63}$$

$C_y \alpha$ is the linearised tyre characteristic and a represents the initialisation transient [5]. The initialisation transient is the time range, given a certain speed, needed for the frictional force to saturate.

An important property of a tyre is its dependence on the wheel load. Although cornering force, at a given slip angle, rises with vertical load it does not rise proportionately with load. The maximum cornering force per unit load occurs at the lightest loads. This can be seen in Figure 2.14 by noticing that the slope of the curve is steeper at lighter loads, assumed a certain side slip angle. The property of increasing side forces at increasing wheel loads is a physical property that will be used in this work to influence the lateral dynamics of a vehicle.

[4]The suffixes are not included in the equations.

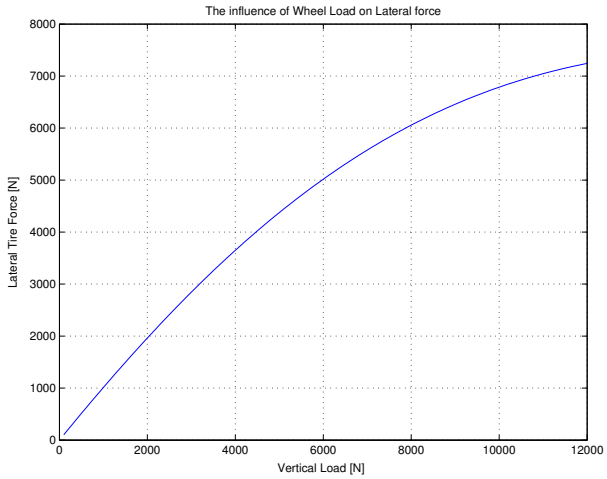

Figure 2.14 Lateral force dependency on the wheel load

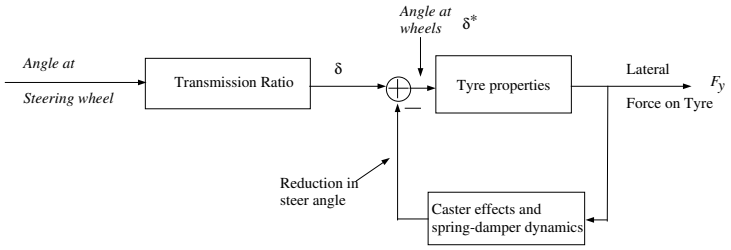

Figure 2.15 Block diagram of Steering system

2.5 Steering system

In previous section the effect of caster and its stabilising effect was mentioned. The side force acting on a tyre creates a moment about the vertical wheel axis which leads to a reduction in the wheel steering angle. This effect can be seen as a feedback as illustrated in Figure 2.15. δ^* is the angle of the wheel.

The steering system is modelled as a mass, spring and damper system. An illustration of this is shown in Figure 2.16. The corresponding equation is 2.64

$$J\ddot{\delta}^* + b\dot{\delta}^* + c\delta^* = -F_y n_L + J\ddot{\delta} + b\dot{\delta} + c\delta \tag{2.64}$$

J is the moment of inertia of the system, whereas b and c are the damp and spring coefficients. It's customary to neglect $\ddot{\delta}$ as input signal, and the two input signals to the steering system is the steering angle (after transmission ratio), δ, and the time derivative of the steering angle (after transmission ratio), $\dot{\delta}$. It is assumed that the driver provides enough torque to the steering wheel to create the steering angle which is used as input. When simulating, a low-pass filter is used to attain the time derivative of the steering angle as shown in Figure 2.17. δ_u is the unfiltered input signal, and δ^* and $\dot{\delta}^*$ are the attained input signals for the model.

2.6 Coupling of the models

When designing controllers for the vertical dynamics, i.e. controllers for the active suspension, only the dynamics described in the vertical model is considered and

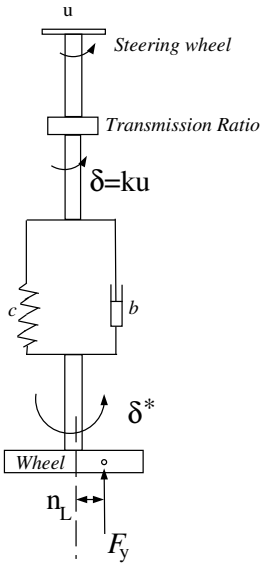

Figure 2.16 Model of Steering system

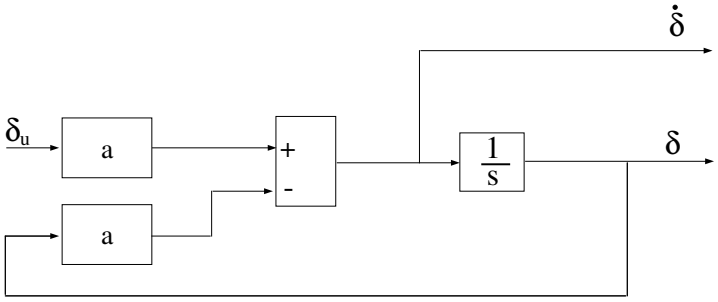

Figure 2.17 Filter for the steering system

the roll and pitch moments that are caused by longitudinal and lateral acceleration are inputs to this model. When designing controllers attenuating the effects of lateral disturbances in yaw rate or side slip angle, the vertical dynamics are not considered. Since the coupling that exists between vertical and lateral dynamics had to be considered in this work, the models were coupled.

The longitudinal and lateral accelerations creates moments around the roll and pitch axis respectively. These moments alters the distribution of how the vertical forces are acting upon the vehicle. E.g. during cornering, parts of the vertical forces acting on the tyres, will be transferred from one side of the vehicle to the other. Since the tyres capability of producing lateral forces are dependent on the vertical forces, the lateral forces acting on the vehicle will change. This *loop effect*, is illustrated in Figure 2.18. The tyres, the steering system and the four-wheeled vehicle models are all a part of the horizontal model.

The lateral acceleration acting on the center of gravity causes a roll motion of the vehicle. The roll axis is moving during cornering and it is also tilting from a higher position rear to a lower position front. In this work, the roll axis has for simplicity been assumed to be fixed, and in a horizontal plane as shown in Figure 2.19. The calculation of the roll moment that acts on the vertical model is done according to equation 2.65. The changes in vertical load are calculated as an

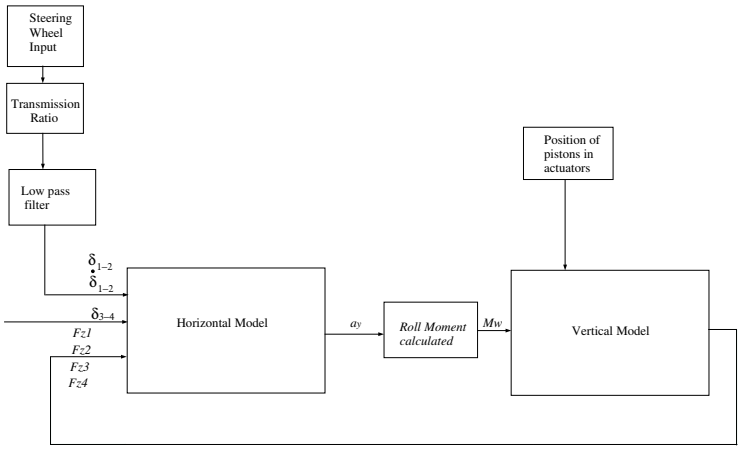

Figure 2.18 Connection between the models

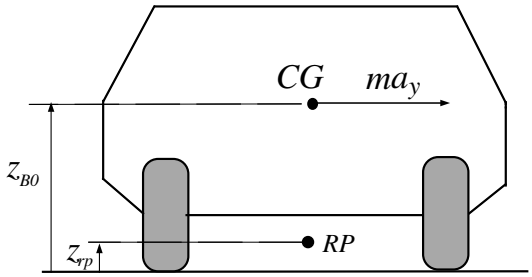

Figure 2.19 The lateral acceleration is causing a roll motion of the car body

ordinary force-spring equation, 2.66.

$$M_r = ma_y(z_{B0} - z_{RP}) \tag{2.65}$$

$$F_{Zi} = -c_W(z_{Wi} - w_i) \tag{2.66}$$

2.7 Aerodynamics

The air surrounding a vehicle exerts on any point of its surface a force per unit area. This force consists of one pressure force, acting perpendicular to the surface, and one tangential force, laying in the plane tangent to the surface. The tangential

Table 2.4 Variables and constants for Aerodynamics

ρ	Air density
A	Reference surface
v	Absolute wind velocity
l	Distance between front and rear wheels

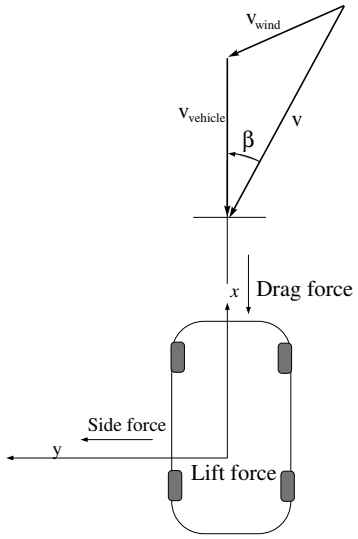

Figure 2.20 Aerodynamic forces acting on a Vehicle

force is due to the viscosity of the fluid. All these forces are integrated over the area and the resulting forces and moments are applied in the center of gravity. The moments arise from the fact that the forces do not act on the center of gravity but at the center of pressure which varies with the stream angle of the air. The flow exert forces and moments about all three coordinate axles.

The generalised equations obtained by experimental testing are expressed as equation 2.67 and equation 2.68. These equations arise from the assumption that the forces and moments are proportional to the dynamic pressure of the free current, $\frac{1}{2}\rho v^2$, to a reference surface, A, and to a reference length, l. The non-dimensional shape factors, c_F and c_M are dependent on the stream angle and the shape of the vehicle, see Figure 2.20 and they have been computed taking the reference surface and reference length into account. When determining the shape factors for a vehicle, they are determined about all three axes as a function of the stream angle, $c_F = c_F(\beta)$ and $c_M = c_M(\beta)$.

$$F = \frac{1}{2}\rho c_F A v^2 \tag{2.67}$$

$$M = \frac{1}{2}\rho c_M A v^2 l \tag{2.68}$$

Heavy side winds alters the behaviour of the vehicle. If the strength of a wind gust is very high the results can be severe if the driver is not alert. Weaker side winds are more of an annoying factor than a critical one.

2.8 Linearisation

Since the vertical model described in an earlier section is already linearised the equations to be linearised are the ones describing the lateral dynamics and the tyres.

$$m(\dot{v}_x - v_y\dot{\psi}) = \sum_{i=1}^{4}(F_{xi}\cos\delta_i - F_{yi}\sin\delta_i) \tag{2.69}$$

$$m(\dot{v}_y + v_x\dot{\psi}) = \sum_{i=1}^{4}(F_{xi}\sin\delta_i + F_{yi}\cos\delta_i) \tag{2.70}$$

$$I_{zz}\ddot{\psi} = \sum_{i=1}^{4} h_i(-f_{xi}\sin\theta_i + f_{yi}\cos\theta_i) \tag{2.71}$$

$$\dot{F}_{yi} = \frac{v_{xi}}{0.03v_{xi} + 0.5}\left(C_y\alpha_i - F_{yi}\right) \tag{2.72}$$

When linearising the equations above, the longitudinal acceleration is assumed to be zero and this equation isn't used. The equations of the steering system is included in the lateral state space model and the state- and input vectors used in the linearisation ($\dot{x} = Ax + Bu$) are:

$$x = \begin{pmatrix} \delta_1^* & \dot{\delta}_1^* & \delta_2^* & \dot{\delta}_2^* & v_y & \psi & \dot{\psi} & F_{y1} & F_{y2} & F_{y3} & F_{y4} \end{pmatrix}^T \text{ and} \tag{2.73}$$

$$u = \begin{pmatrix} \delta_1 & \dot{\delta}_1 & \delta_2 & \dot{\delta}_2 & \delta_3 & \delta_4 & F_{Z1} & F_{Z2} & F_{Z3} & F_{Z4} \end{pmatrix}^T \tag{2.74}$$

and we arrive at a state space representation for the tyres, the steering system and the lateral dynamics with eleven states and ten inputs.

Eq.2.70 and eq.2.71 are linearised together with eq.2.72

$$\dot{x}_1 = \dot{\delta}_1^* \tag{2.75}$$

$$\dot{x}_2 = \ddot{\delta}_1^* = -\frac{c}{J}\delta_1^* - \frac{c}{J}\dot{\delta}_1^* - \frac{n_L}{J}F_{y1} + \frac{c}{J}\delta_1 + \frac{b}{J}\dot{\delta}_1 \tag{2.76}$$

$$\dot{x}_3 = \dot{\delta}_2^* \tag{2.77}$$

$$\dot{x}_4 = \ddot{\delta}_2^* = -\frac{c}{J}\delta_2^* - \frac{c}{J}\dot{\delta}_2^* - \frac{n_L}{J}F_{y2} + \frac{c}{J}\delta_2 + \frac{b}{J}\dot{\delta}_2 \tag{2.78}$$

$$\dot{x}_5 = \dot{v}_y = -v_x\dot{\psi} + \frac{1}{m}\sum_{i=1}^{4}(F_{xi}\sin\delta_i + F_{yi}\cos\delta_i) + \frac{1}{m}F_y^d \tag{2.79}$$

$$\dot{x}_6 = \dot{\psi} \tag{2.80}$$

$$\dot{x}_7 = \ddot{\psi} = \frac{1}{I_{zz}}\sum_{i=1}^{4} h_i(-f_{xi}\sin\theta_i + f_{yi}\cos\theta_i) + \frac{1}{I_{zz}}M_z^d \tag{2.81}$$

$$\dot{x}_i = \dot{F}_{y(i-7)} = \frac{v_{x(i-7)}}{0.03v_{x(i-7)} + 0.5}\left(C_y\alpha_{(i-7)} - F_{y(i-7)}\right), i = (8, ..., 11) \tag{2.82}$$

For simulation purposes, disturbances (e.g. wind disturbances) are added to the lateral model. In equation 2.79 and equation 2.81, F_y^d and M_z^d have been included. The lateral and vertical models are coupled as shown in Figure 2.18 and integrated into one state space model where the external disturbances F_z, M_r and M_p were removed. By doing this, it is assumed that the disturbances caused by the wind in these degrees of freedom can be neglected. The total state and input vectors are:

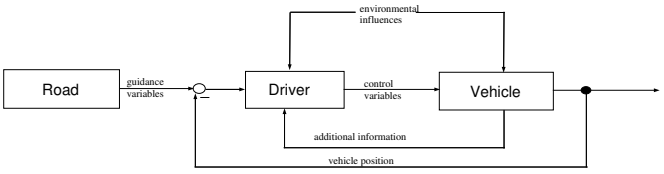

Figure 2.21 Driver-environment control loop

$$x = \begin{pmatrix} \delta_1^* & \dot{\delta}_1^* & \delta_2^* & \dot{\delta}_2^* & v_y & \psi & \dot{\psi} & F_{y1} & F_{y2} & F_{y3} & F_{y4} & z_B & \dots \\ \dots & p & r & \underline{z}_W & \dot{z}_B & \dot{p} & \dot{r} & \dot{\underline{z}}_W \end{pmatrix}^T \tag{2.83}$$

$$u = \begin{pmatrix} \delta_1 & \dot{\delta}_1 & \delta_2 & \dot{\delta}_2 & \delta_3 & \delta_4 & \underline{u} & \underline{w} & F_y^d & M_z^d \end{pmatrix}^T \tag{2.84}$$

The system was linearised numerically in Matlab, and the system is simulated in Simulink. To determine the matrices of the linearised system the point about which the system is to be linearised must be given. The linearisation program takes the four wheel angles $(\delta_1, ..., \delta_4)$ as input, as well as the yaw rate, $\dot{\psi}$ and the longitudinal and lateral velocities, v_x and v_y. The tyre forces can be calculated knowing these values[5]. When linearising about a point which gives a longitudinal acceleration that differ from zero this fact has to be compensated for (since we've assumed constant velocity). In the linearisation program a routine has been written that minimises the absolute value of the resulting longitudinal force (using Newton-Raphsons method) changing the rear wheel angular velocities. This routine increases the angular velocities at the rear wheels thus creating larger longitudinal forces[6].

2.9 Non-linear simulation model

Today's development of automotive vehicles strongly rely on the use of computer simulations in the design of new vehicles. The aim of computer models is to reveal, as early as possible in the design phase, the effect of new components on the vehicle dynamics when operating together with the existing systems. At Daimler-Chrysler AG, a simulation package called CASCaDE (Computer Aided Simulation of Car, Driver and Environment) has been developed. This package includes a number of different vehicle models and also models of drivers and environments (see Figure 2.21). Data files describing the characteristics of different components of the vehicle are collected in this package and these are put together with dynamical equations which may be linear or non-linear. This package has been used extensively throughout this work as a reference for parameters, as a validation tool for the vehicle model that can be linearised and as a tool for evaluating the designed controller.

[5] See Appendix A

[6] Assumed that the slip won't grow large enough for the forces to start decrease again.

3. Validation

3.1 Introduction

Once the model is constructed, it should be verified with information from the real system, that the model is acceptable. Since the construction of a model involves many simplifications, there are deviations in model outputs compared to tests performed on a real plant. A common method of model validation is to compare simulation results to actual measurements.

Because of the highly nonlinear nature of a vehicle, the vehicle model derived in previous chapter cannot be used for certain manoeuvres. The main reason for this is due to the nonlinearities of the tyres. The kinds of manoeuvres for which the model is valid will be discussed in this chapter. Further, a comparison between simulation results from the linearised model where the parameters have been have been adjusted and CASCaDE will be shown. Also tests performed on the Technoshuttle will be compared to simulations from the vehicle model which was linearised.

3.2 Validation of Vehicle Model

Many of the parameters used in the vehicle model have been taken from CASCaDE. These values gives an idea about in what range the parameters should be in the model that can be linearised. By adjusting the values of the parameters for the linearised model, a better model match can be attained. The tuning of the parameters where done with a bit of a-priori knowledge.[1]

Figure 3.1, 3.2, 3.3 and 3.4 shows simulation results from a saturated ramp (almost a step) in the steering wheel angle. The slope of the input signal is 500 degrees per second and the saturation point is 30 degrees (turning left), driving at a speed of 80 km/h. In this simulation, the ABC system was switched off, hence the oscillations in wheel load and roll rate. The steady state gains are fairly accurate but there are clearly deviations in the comparison.

Figure 3.5 and 3.6 displays a similar manoeuvre but with a saturation point of 45 degrees and having the ABC controller activated. The similarity decreases with increasing saturation point and at about 60 degrees, the deviations start to become even more significant.

One of the main objectives of this work was to analyse how the active suspension could be used to influence the lateral dynamics. This will be described more thoroughly in following chapter. However, a simulated step in warp will be compared to a test performed with the Technoshuttle. When applying warp to a vehicle, vertical forces are applied on a pair of diagonal wheels as illustrated in Figure 3.7. The change in vertical forces on the wheels are made possible due to the suspension actuators. The vertical wheel forces causes the vehicle to turn since a yaw moment is created.

It's not possible to use the position of the pistons as inputs to the test vehicle and therefore the dynamics of the actuators are necessary for the vehicle model. In [6] and in CASCaDE, the dynamics of the suspension systems actuators are modelled as in equation 3.1, where T_a and K_a are diagonal matrices and $\underline{i}$ is a vector containing the currents to the actuators.

[1] It may be possible to attain a better model using an identification program which optimizes parameters.

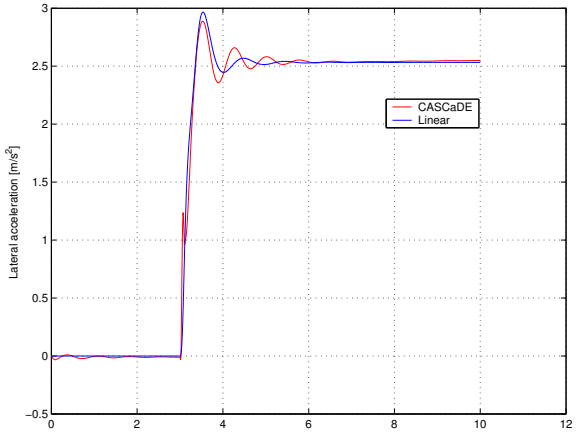

Figure 3.1 Lateral acceleration at a 30 degrees saturation point

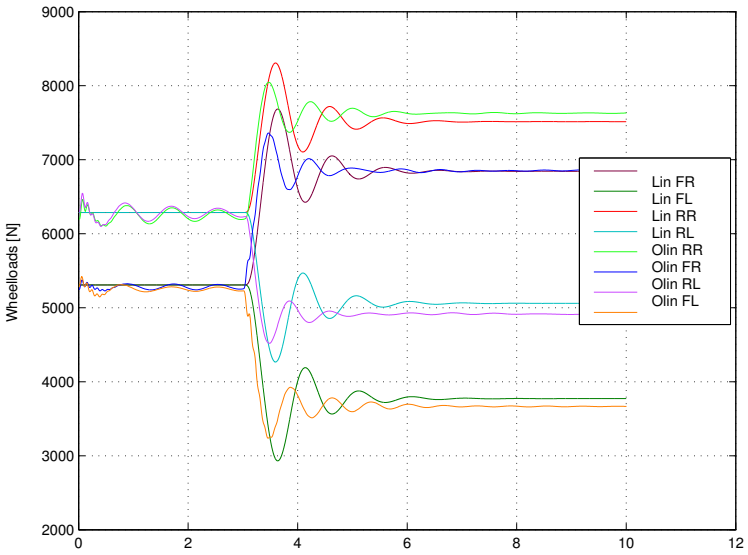

Figure 3.2 Wheel Loads at a 30 degrees saturation point

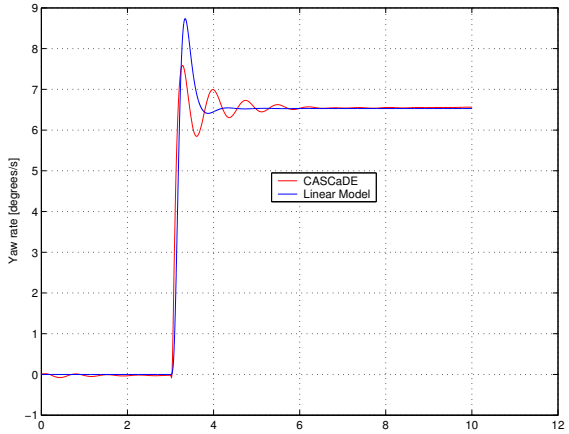

Figure 3.3 Yaw Rate at a 30 degrees saturation point

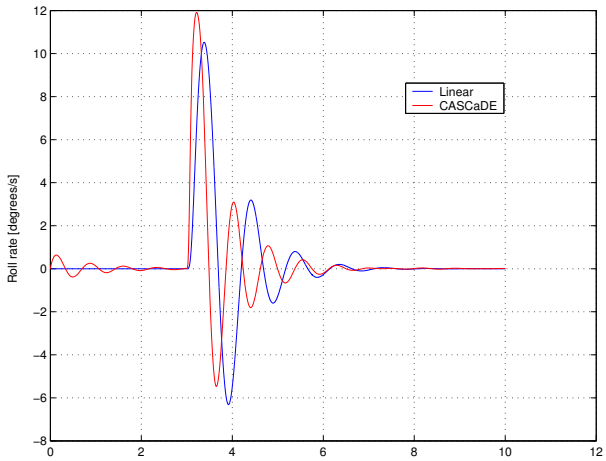

Figure 3.4 Roll Rate at a 30 degrees saturation point

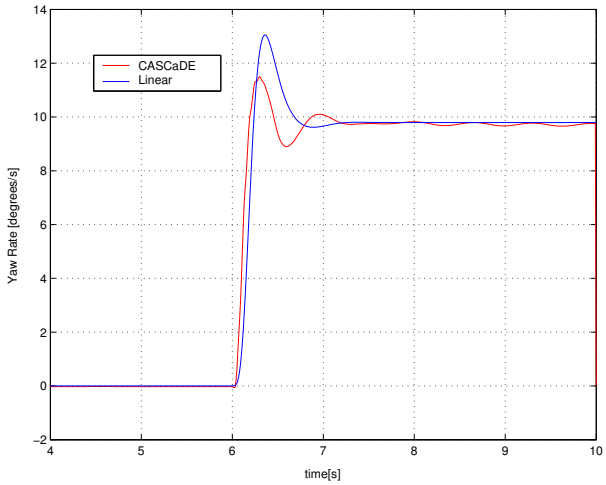

Figure 3.5 Yaw Rate at a 45 degrees saturation point

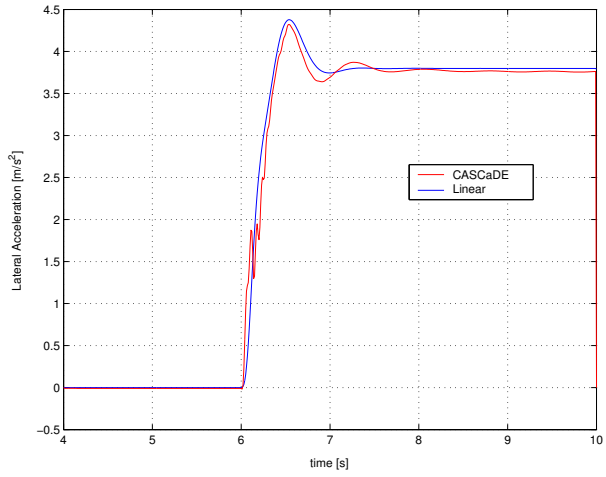

Figure 3.6 Lateral acceleration at a 45 degrees saturation point

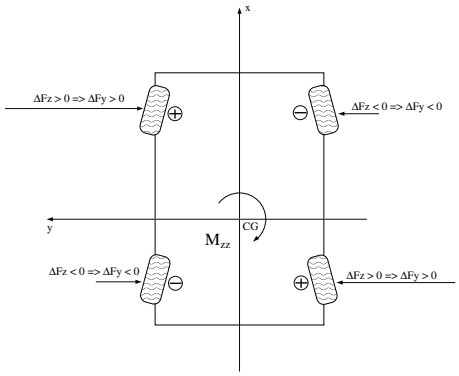

Figure 3.7 Warp effect

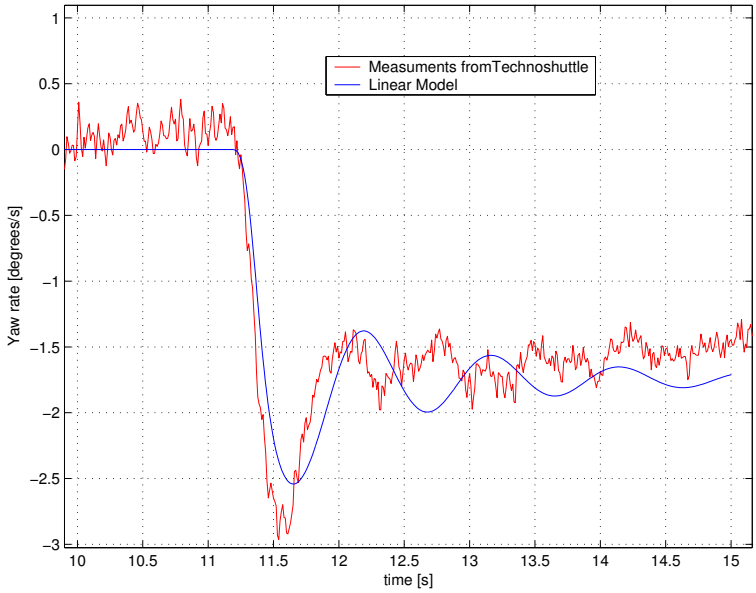

Figure 3.8 Yaw rate due to warp at test without ABC

$$T_a \dot{\underline{u}} + \underline{u} = K_a \int_{t=0}^{t_{end}} \underline{i} dt \tag{3.1}$$

If transformed into frequency domain we get:

$$\underline{u} = (T_a s + I_4) K_a \frac{1}{s} \underline{i} \tag{3.2}$$

Figure 3.8 shows the resulting yaw rate that is achieved driving at 100 km/h and applying an input signal to the actuators of 1000 mA for 0.15 seconds[2]. There are quite heavy oscillations in this test since the ABC system wasn't activated. In Figure 3.9 a comparison between the linearised model and CASCaDE is shown. Warp has been applied having the ABC system activated. The applied forces to the suspension struts were ±5400 N front and ∓3000 N rear.

[2]The toe in angle on the front wheels are approximately 0.2 degrees and 1.0 degrees on the rear wheels.

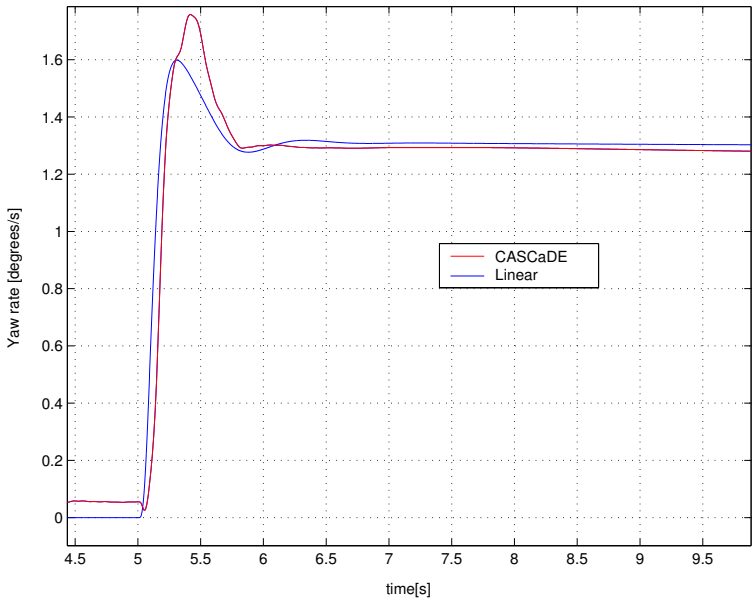

Figure 3.9 Yaw rate due to warp at simulation with ABC

3.3 Limitations of Linearised model

As can be seen in the comparisons in previous section there are deviations compared to tests on the vehicle and to simulations performed in CASCaDE. The steady state values are fairly accurate but the main deviations are in the phase. Particulary in comparisons between cornering manoeuvres, it can be seen that the frequency of the oscillations in the linearised model tend to be lower than in CASCaDE simulations. The most important manoeuvre to be as accurate as possible is when warp is applied. Figure 3.9 displays a satisfactory accuracy for being able to continue with control design and analysis.

Certain simulation manoeuvres will not display a good match to real measurements. One standard manoeuvre when evaluating a lateral vehicle model, is to drive straight ahead and apply a ramp signal to the steering wheel up to a specified limit where it will saturate. If this limit is set too high, the linear tyre model will not be valid and the simulation results will not be acceptable. Since the vehicle model assumes constant velocity, manoeuvres involving big changes in velocity such as braking and acceleration, will not display acceptable results. Another evaluation manoeuvre is to apply a sine wave to the steering wheel. This manoeuvre showed acceptable similarities to CASCaDE provided that the amplitude of the input signal wasn't too big.

The main objectives of the model is for analysis and control design purposes. The possibility of re-tuning a controller in CASCaDE exists and the model will at least give a reasonable indication of, what direction to take when designing the controller.

4. Analysis of Vehicle side wind compensation

4.1 Introduction

In this chapter some different possibilities of rejecting wind gusts will be presented with the focus kept on using the active suspension system. The mechanisms that makes steering by warping possible will also be presented, as well as to what extent the effects from warp can be used for attenuating wind gusts.

4.2 Possibilities of side wind compensating

There may be a number of different solutions when it comes to rejecting side wind. Below, a few are mentioned:

- *The steer by wire system* (SBW), has been evaluated in earlier work, (see i.e.[3]), and tests were performed with the Technoshuttle. The results of the tests can be seen in Figure 4.1. Both the yaw rate and side slip angle where reduced[1].
- *Rear Wheel Steering*
- *Steering wheel assistant*, is to be implemented into some of the newer Mercedes models and the main idea, is to assist the driver in steering, by applying a torque to the steering wheel axle, leaving the option for the driver to maintain the steering angle.

[1]The side wind is coming from the right and since the center of pressure is located in front of the center of gravity, a positive yaw moment is created.

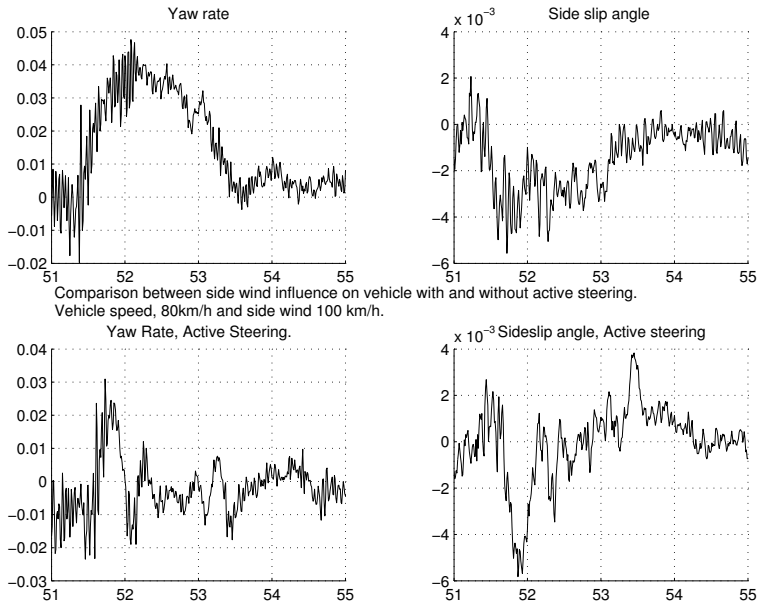

Figure 4.1 Side wind rejection using SBW.

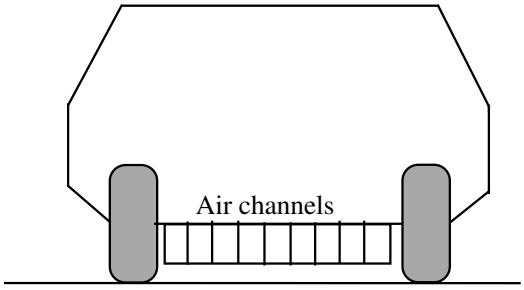

Figure 4.2 Side wind rejection using Air channels.

- *Aerodynamic effects*, similar to what is used in aircrafts, may be possible to use to reduce the effect of a wind gust. If a number of air channels (see Figure 4.2), which can be opened and closed, are mounted onto the body, the channels can be used for creating aerodynamic pressure forces which gives rise to a yaw moment. If the forces are big enough, the channels can be used for side wind rejection.
- *Sensotronic Brake Control*, (SBC) includes control systems such as ESP (Electronic Stability Program) and ABS (Anti-lock Braking System). The SBC can be used for creating longitudinal forces on the tyres, thus stabilising the vehicle in case of a wind gust as in Figure 4.3. By using the SBC the driver may experience a reduction in comfort, but this has to be further analysed.

4.3 Steering by warping

With the active suspension system, it is possible to influence the roll, the pitch and the lift of the chassis as was shown in the modelling chapter. Since the vehicle has four wheels and sofar only three properties have been considered, it is overdetermined. This makes it possible to introduce a fourth property, the warp. Warp is defined as $\Omega = F_{z1} - F_{z2} - F_{z3} + F_{z4}$, i.e. the difference in wheel load on the front axle minus the difference in wheel load on the rear axle.

Different mechanisms are contributing to the effect warp has on the steering behaviour of a vehicle. Two different mechanisms that have influence will be described here. Firstly, the change in steering angle due to roll on an axle which is induced by the actuators in the suspension struts. Secondly, the influence from the pre-set toe in.

Firstly, when roll is applied to an axle by the active suspension system, a change in the wheels steering angle occurs due to the mechanics of the wheels bearing system and due to the forces acting on the tyres. The roll angle on an axle can be set within certain limits corresponding to the saturation points of the suspension systems actuators. Tests have been performed on the Technoshuttle

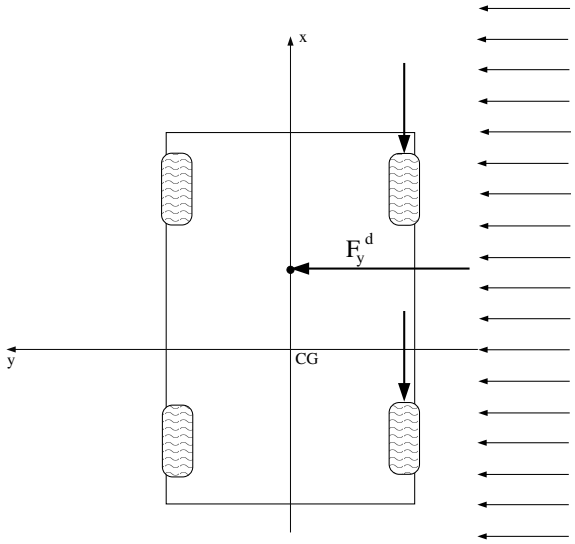

Figure 4.3 Side wind rejection using SBC.

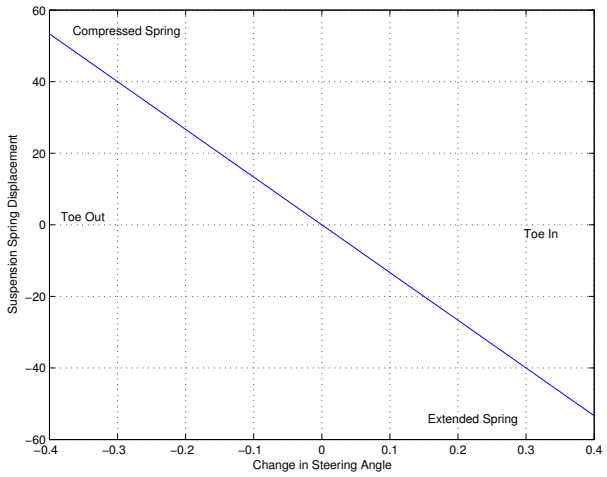

Figure 4.4 Change in steering angle in relation to suspension spring displacement.

and these show the relation between suspension spring displacement and change in steering angle on an axle. These tests have shown that the relationship between the roll angle and the change in the steering angle of the wheels are fairly linear and an illustrating curve is shown in Figure 4.4.

If applying warp to a vehicle, there is a roll motion in one direction on the front axle and a roll motion in opposite direction on the rear axle. These roll motions causes the angles of the wheels to change. Since there is a change in wheel angle, the wheel slip also changes thus creating side forces on the tyres. Since there is no longer symmetry in the side forces, a yaw moment is creates. The maximum roll angle corresponds to the limits on the spring displacements, and this roll angle corresponds to the maximum change in steer angle.

As previously mentioned, the lateral force a tyre can produce is dependent on the vertical load on the wheel. If forces are applied to the suspension struts, as shown in Figure 4.6, the lateral force on a wheel initially increases with increasing wheel load, provided that the angle of the wheel is different from zero. These lateral forces creates a yaw moment. Simulations showed that the greatest effect

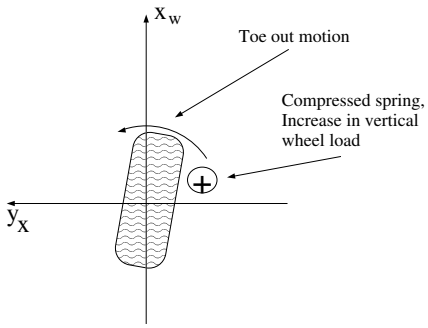

Figure 4.5 The toe out motion that occurs due to compressed suspension spring.

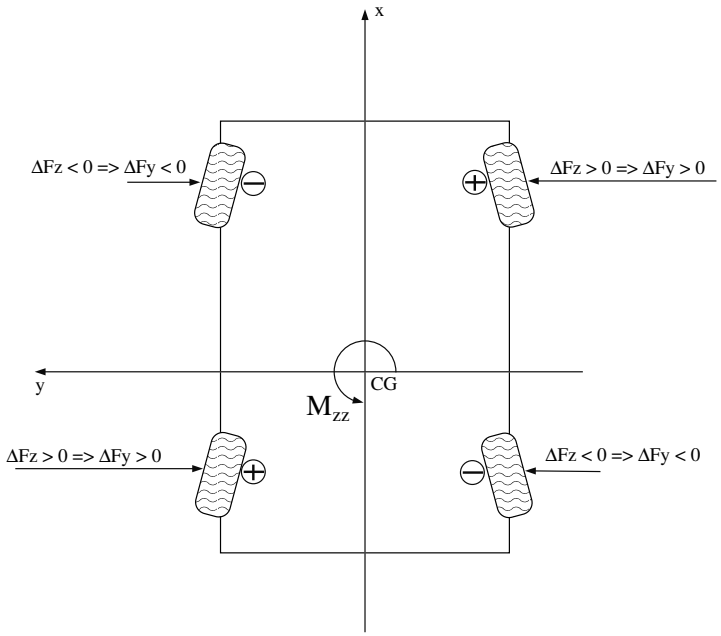

Figure 4.6 Toe in on a vehicle.

comes from the pre-set toe in angles. This is shown in Figure 4.7 where a step in warp has been applied. The values of the toe ins are 0.4 degrees on the front wheels and 1.0 degrees on the rear wheels. These values are greater than the values set on the usual vehicle, but since the toe in angles on the rear axle easily can be set to 1.0 degrees they are reasonable to work with. The influence on the yaw rate coming from the roll motion on the axles, counteracts the contributing effect from the toe in. Because of this, the yaw rate initially goes in opposite direction.

4.4 Simulations and tests of warp effects

Tests performed on the Technoshuttle and simulations done in CASCaDE show that the greatest influence on the yaw moment is due to the toe in angle on the rear axle. The values shown in Figure 4.8 are the maximum yaw moment values created during warp and varying the toe in angles on front and rear axle

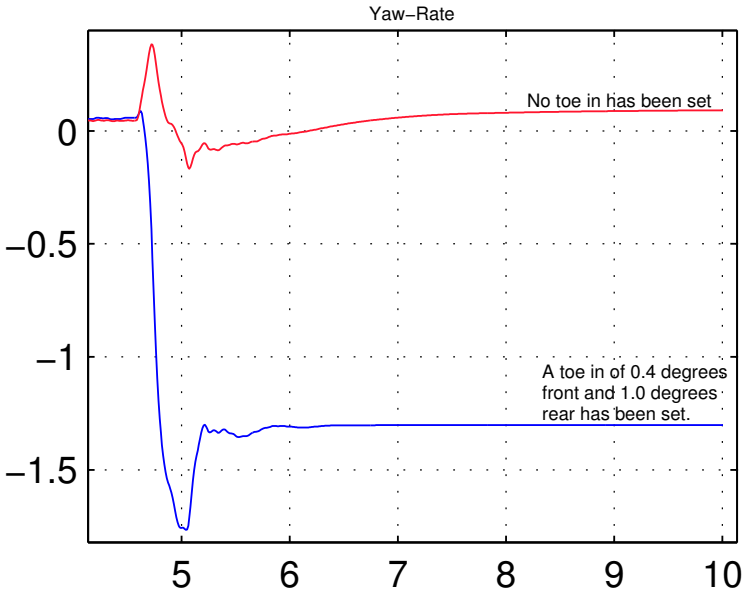

Figure 4.7 Effect of toe in on yaw rate.

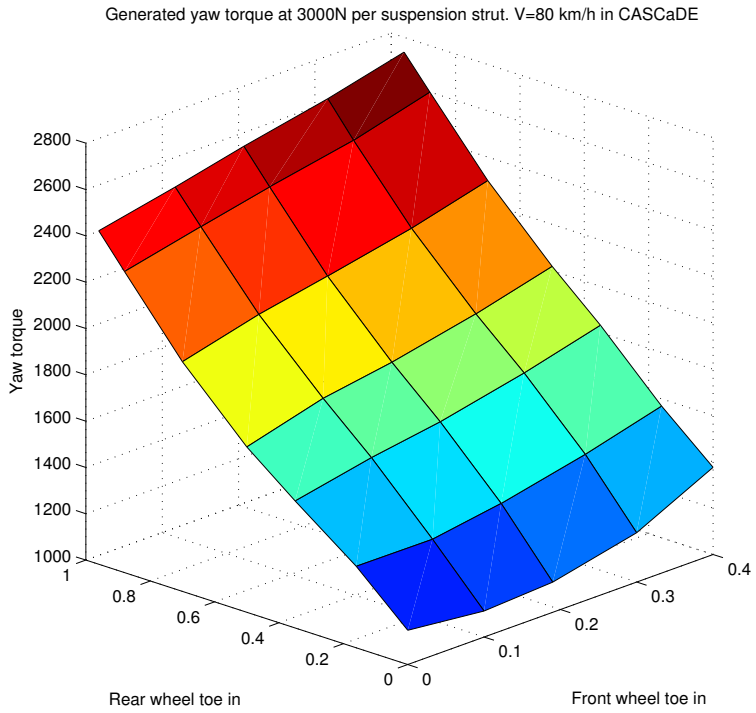

Figure 4.8 Peak Yaw Moment at different toe ins.

respectively. When simulating warp with the toe in on the front axle with 0.4 degrees and on the rear axle with 1.0 degrees and varying the velocity as in Figure 4.9, we can see that the generated yaw moment increases with velocity. The reasons for this have yet to be identified.

In Figure 4.10 warp [2] has been applied and a yaw moment was created, but

[2]In this case negative warp, driving at 80 km/h with a front toe in of 0.4 degrees and 1.0 degrees rear. The forces on the front suspension struts were ±5400 N and on the rear suspension struts ∓3000

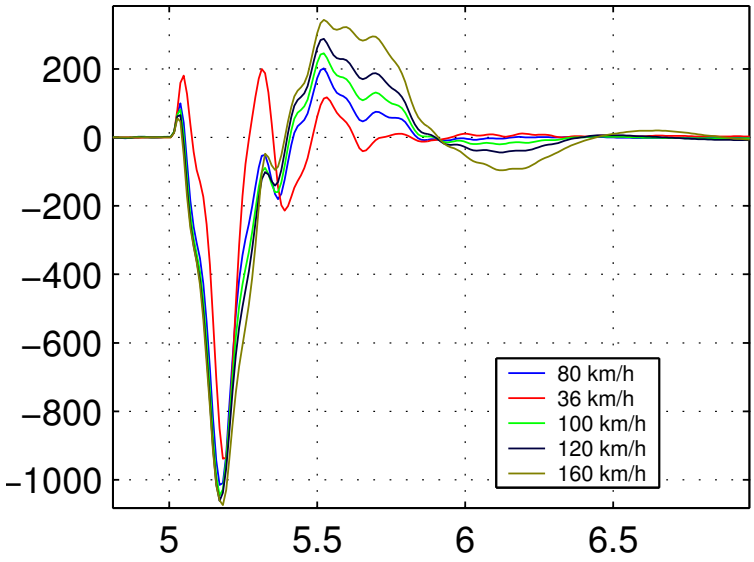

Figure 4.9 Yaw Moment at different velocities.

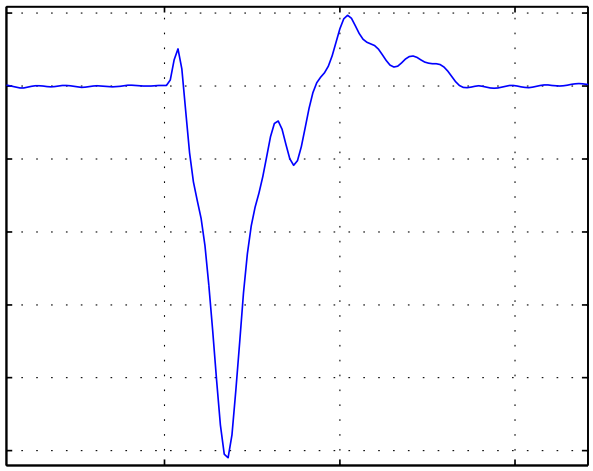

Figure 4.10 Yaw Moment during warping.

only for a short period of time. The effect warp has on the yaw moment is only instantaneous. The main reason for this is the increasing tyre side slip angle on the rear left tyre and the decreasing tyre side slip angle on the rear right tyre. The lateral forces on the rear left tire increases due to the increasing tyre side slip angle. This can be seen in Figure 4.11. The corresponding side forces on front axle, $F_{y1} + F_{y2}$ and rear axle,$F_{y3} + F_{y4}$ are illustrated in Figure 4.12, and that the rear axle produce the desired force only for a quarter of a second.

The phenomenon can be explained with the help from Figure 4.13. By increasing the forces on the suspension struts, point 2 should be reached. But since there is a change in the tyre side slip angles we actually end up in point 3, thus creating side forces on the rear tyres that stabilises the yaw motion. The increasing tyre side slip angle on the rear left tyre is due to the toe out motion that occurs at this wheel (extended spring), and due to the increasing lateral velocity on the rear axle which arises when a negative yaw motion is present.

N.

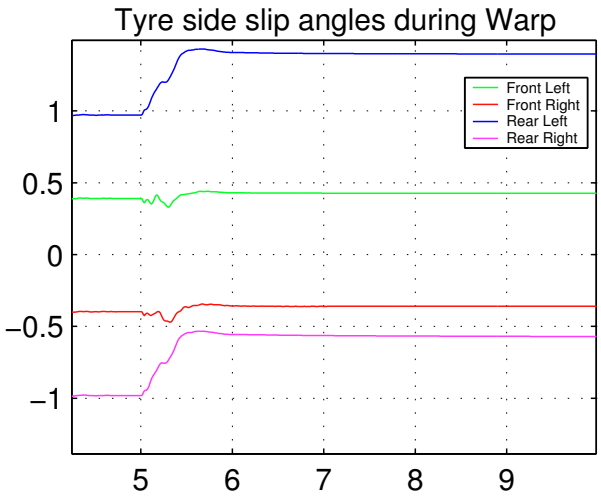

Figure 4.11 Tyre side slip angles during warp.

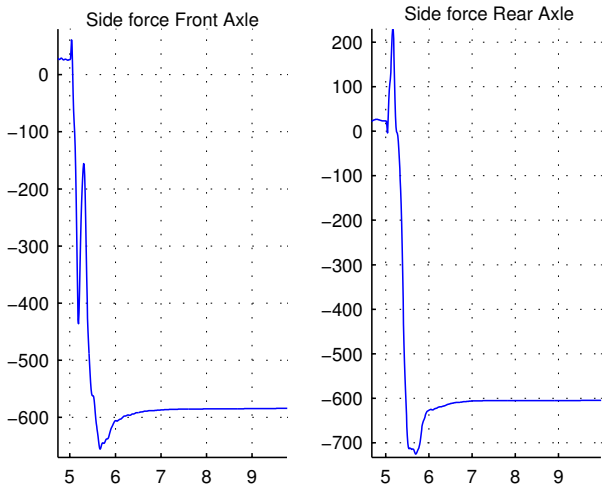

Figure 4.12 Side forces on the axles during warp.

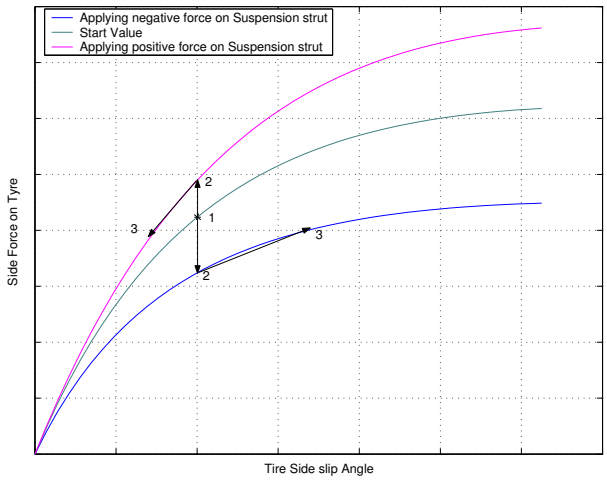

Figure 4.13 Lateral forces on tyres during warp.

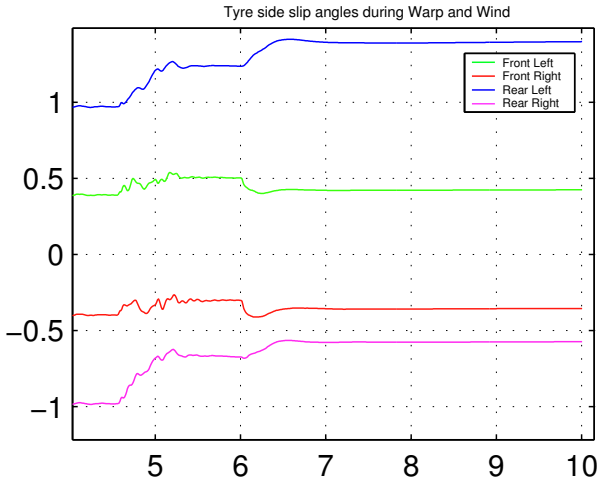

Figure 4.14 Tyre side slip angles at a wind gust applying warp.

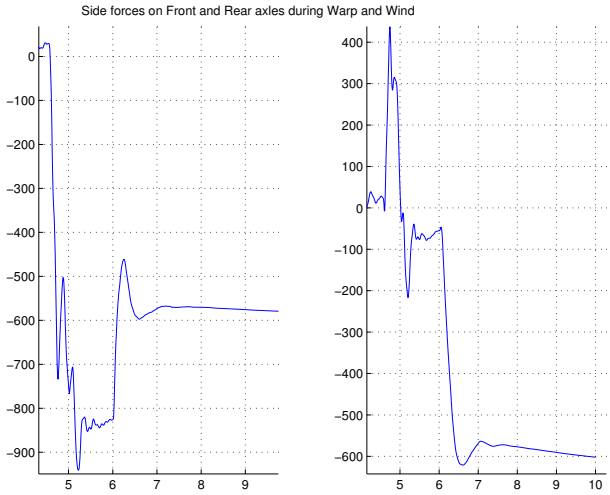

Figure 4.15 Side forces on the axles during warp and wind.

The same simulations were performed, but applying a wind gust of 20 m/s in positive lateral direction at the same instant as warp is applied. In Figure 4.14 it can be seen that the side slip angles of the tyres (which counteract the yaw moment) are less than when just applying the warp. Figure 4.15 shows the corresponding side forces on front and rear axle.

It can then be concluded that the yaw moment produced by the tyres remains, as long as the wind is present. The moment is greater at first, but is slightly reduced when the tyre side slip angles on the rear wheels have been built up, and the main contribution comes from the front axle. The positive lateral force on the rear tyres remains during a part of the wind gust but it never decreases to the corresponding value without side wind.

Consequently, the use of warp for steering the vehicle without lateral disturbances, is limited, but for attenuating wind gust effects, warping the vehicle can be used to some extent, provided the toe in angles are big enough. Further, tests performed using the Technoshuttle, showed that the vehicle during braking is undriveable, since the vehicle then becomes unstable. This means that warp can only be applied for a short period of time and that it can only be used for side wind compensation when driving without braking and when the angle of the steering

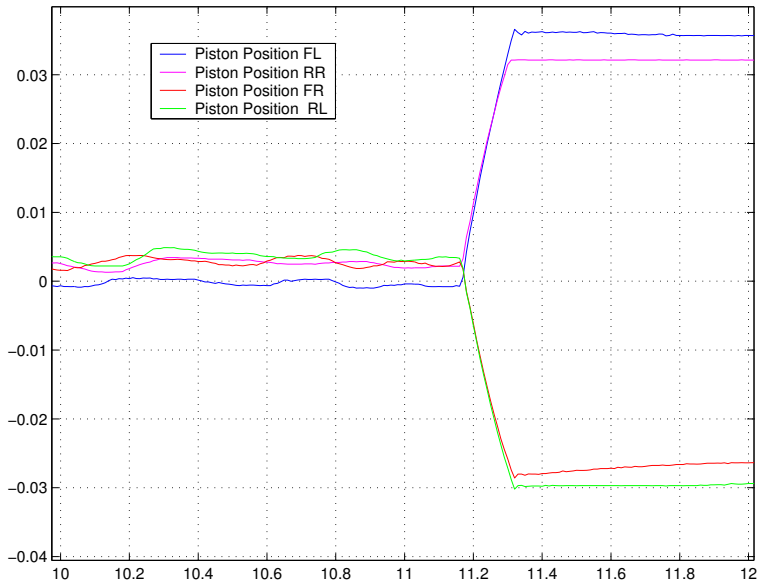

Figure 4.16 The actuator response to a 0.15 s 1.0 A impulse on every actuator

wheel is close to zero.

4.5 Actuator performance

If using the ABC system for controlling lateral disturbances, it is required that the actuators of the suspension system are sufficiently fast. Therefore, the actuators were tested and the responses of a current impulse on every actuator can be seen in Figure 4.16.

It is concluded that the actuators are fast enough by first comparing the real measurements with simulation results, and then simulate a step in warp at the same instant as a wind gust is applied. It is then the task of the controller to make certain that the appropriate action is taken fast enough.

When applying warp to the vehicle, it is not desirable to reach the limits of the actuators. When wind is acting on the vehicle there is a change in roll angle, thus generating forces to the suspension struts from the comfort controller in the ABC system[3]. Therefore, it's not possible to fully use the actuators during side wind compensation, since the comfort controller needs space to work. However, during the simulations in this chapter this was taken into account.

4.6 Evaluation of Side Wind Compensation using warp

Simulations have shown, that when applying the maximum step in roll angle, a greater yaw rate can be generated than when applying the maximum step in warp (this will not be shown here). However, by using a roll motion, the comfort the driver experiences is decreased. The roll angle is applied very quickly and the resulting roll angle is between three and four degrees. By using warp, a lesser effect is achieved, but without causing a significant increase in roll, pitch or lift motion.

The maximum warp that can be applied, doesn't fully compensate for the yaw rate that is caused by a heavy wind gust. Wind gusts that are slower than 14

[3]See Chapter 5

m/s are possible to compensate for, assumed that the toe in angles are set to 0.4 degrees front and 1.0 degrees rear when driving at a speed of 80 km/h.

5. Control Design

5.1 Introduction

To implement a warp controller into the existing ABC system, some changes had to be made. In this chapter, the existing ABC system will be described. The transfer function from warp to yaw rate that has been extracted from the linearised vehicle model will be analysed. With this transfer function a PID controller is designed. The PID controller was then evaluated with respect to wind gusts in CASCaDE.

Throughout this chapter it is assumed that the wind can be observed and as previously mentioned the controller can only be used when driving straight ahead without accelerating or braking. The analysis will be carried out for a velocity of 80 km/h.

5.2 Existing ABC system

There are a number of sensors in the vehicle. Two of the sensors measure the longitudinal and lateral accelerations of the body and three sensors measure the vertical accelerations in three points of the body. There are also sensors for the suspension spring displacements and for the positions of the pistons. With these signals it's possible to calculate the roll and pitch angles as well as lift and their accelerations using kinematical relations. The forces in the suspension struts are also calculated. This is done in the *Adapting Signals* block in Figure 5.1. In the second block, *Filter and Comfort Controller*, the signals are first filtered and then the comfort controller, which consists of different feedback controllers, generates force reference values to the force controller. The task of the *Force Controller* is to generate currents to the actuators corresponding to the reference values in force set by the comfort controller.

The structure of the comfort controller is illustrated in Figure 5.2.

It is desirable to control the roll and pitch angles as well as the vertical position of the body and their corresponding accelerations. Since it's not possible to control two states with one input independently of each other, a decoupling is made in frequency domain [7]. E.g. the vertical position of the chassis is controlled up to frequency of about 1 Hz, whereas the vertical acceleration is controlled in the range between 2 and 10 Hz and the small coupling that exists can be ne-

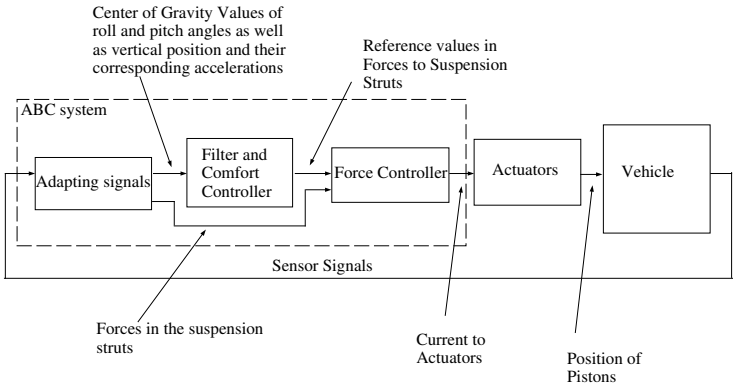

Figure 5.1 ABC system.

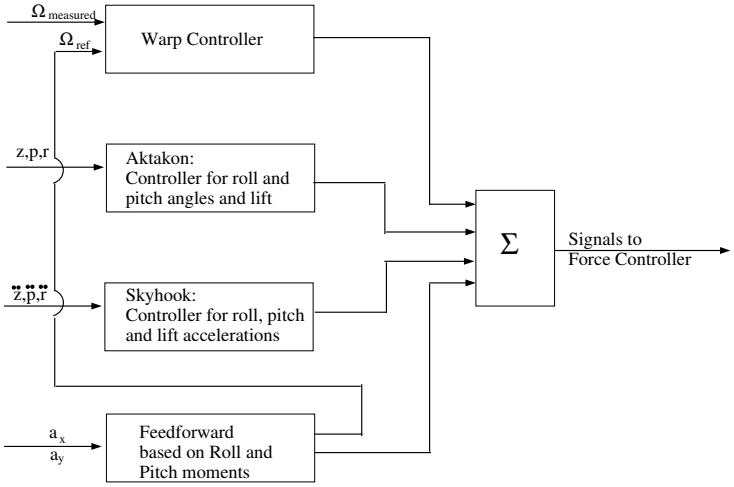

Figure 5.2 Skyhook, Aktakon, Warp controller and Feedforward.

glected. Aktakon, consists of three different feedback controllers with low bandwidth. It compensates for disturbances in roll and pitch angles as well as to lift disturbances. Skyhook, being the high bandwidth compensator, is controlling the corresponding accelerations in roll, pitch and lift.

The input signals to the feedforward, are the longitudinal and lateral accelerations. It acts during manoeuvres where high accelerations are acting on the vehicle, assisting the feedback controllers in keeping the body horizontal.

The warp controller is keeping the warp at zero except when the feedforward is working. It is desirable with zero warp due to its influence on the lateral dynamics. The output of the feedforward generates a warp that differ from zero, and therefore a reference signal is sent to the warp controller to prevent a conflict between the them.

If implementing the designed yaw rate controller into the ABC system, a conflict arises with the existing warp controller which cannot be used because of its low bandwidth. This means that the existing warp controller has to be switched off when the lateral controller is active. In addition, the yaw rate had to be added as input signal to the ABC system.

The dynamics from the force controller input, to the position of the piston in the suspension strut is modelled as a first order system. The amplification is equal to the inverse of the spring constant in the suspension strut, $G_{FCu} = \frac{\frac{1}{c_W}}{\frac{s}{b}+1}$.

The above described ABC system, was implemented into the vehicle model for simulation purposes, and for comparison, the sensor signals were generated from center of gravity values. A derivation of how this is done is presented in Appendix.

5.3 Warp to yaw rate transfer function

It's theoretically possible to apply warp to the vehicle without causing pitch, roll or lift motion[1]. To do this, a more complex model is needed which regards the torsional stiffness and other properties of the chassis. This wasn't considered in this work, but the coupling with roll, pitch and lift was reduced relying on simulations and a bit of analysis. Relying on the equations from the linearised vertical model, there is no coupling between warp and lift or pitch, provided that the warp is

[1]Without having the ABC system activated.

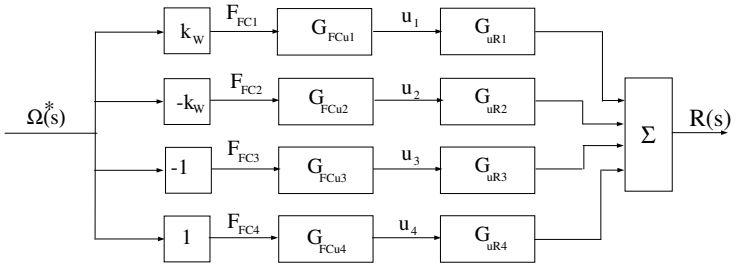

Figure 5.3 Block diagram illustrating the transfer function from the input signal warp to roll angle

applied in such a way that $F_{FC1} = -F_{FC2}$, $F_{FC4} = -F_{FC3}$ and that $F_{FC1} = kF_{FC4}$ for $k > 0$. In this work the warp is applied in such a way that the roll angle is equal to zero in steady state when a step signal is applied. Since there are saturations on the actuators and step signals causes the greatest oscillations, this is the case that was analysed. When applying ramp signals as input, there will be a small roll angle that differ from zero, but as soon as the saturation limits are reached or when the pistons aren't moving, the roll angle will return to zero. The transfer functions from the four positions of the pistons (u_i) to the roll angle can be extracted from the linearised model (5.1).

$$R(s) = \sum_{i=1}^{4} G_{uRi}(s)u_i(s) \tag{5.1}$$

As previously mentioned, simulations showed that first order systems can be used as transfer functions from force controller input, to piston position output. By including the transfer functions from the force controller to the positions of the pistons, equation 5.2 is attained.

$$R(s) = \sum_{i=1}^{4} G_{uRi}(s)G_{FCu}(s)F_{FCi}(s) \tag{5.2}$$

It is assumed that warp is applied in such a way that $F_{FC1}(s) = -F_{FC2}(s)$, $F_{FC3}(s) = -F_{FC4}(s)$ and that the input forces to the force controller front and rear, relate to each other through a weighting factor, i.e. $F_{FC1}(s) = k_W F_{FC4}(s)$. By doing this, the *input signal warp*, can be defined as the convenient scalar, Ω^*, as illustrated in Figure 5.3.

$$\begin{aligned}\lim_{t\to\infty} r(t) = \lim_{s\to 0} sR(s) = \lim_{s\to 0} s(k_W G_{FCu1}(s)G_{uR1}(s) - k_W G_{FCu2}(s)\cdot \\ \cdot G_{uR2}(s) - G_{FCu3}(s)G_{uR3}(s) + G_{FCu4}(s)G_{uR4}(s))\Omega^*(s) = 0\end{aligned} \tag{5.3}$$

By applying the final value theorem, requiring that the roll angle is zero in steady state when a step signal is used as input $\Omega^*(s) = \frac{1}{s}$, it's possible to solve for the weighting factor k_W. The weighting factor is dependent on velocity and is assigned the sign so that positive warp generates positive yaw rate in steady state. The weighting factors differed slightly between the linearised model and CASCaDE, approximately one percent at 80 km/h. In Figure 5.4, the stars corresponds to weighting factors tuned in CASCaDE and the curve is a linear least square fit of these values (equation 5.4, where v is in km/h).

$$k_W(v) = 0.005334v + 1.369 \tag{5.4}$$

By applying the warp in this manner, the maximum step in warp corresponds to a peak in roll angle of 0.45 degrees with a maximum angular velocity of 3

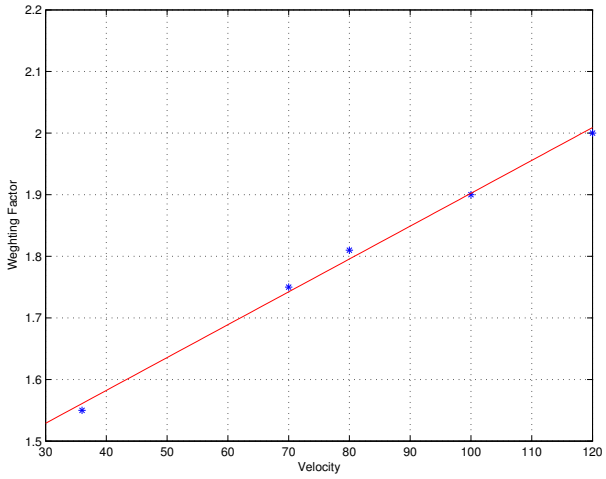

Figure 5.4 Weighting Factor as a function of Velocity [km/h]

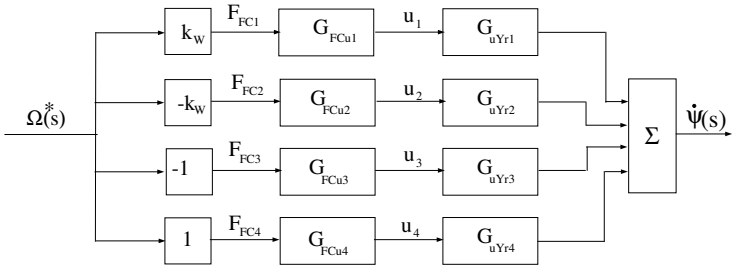

Figure 5.5 Block diagram illustrating the transfer function from warp to yaw rate

degrees per second driving at 80 km/h. The time it takes for the roll angle to return to 0 is around half a second. By doing this, the conflict with other control loops in the ABC system is kept to a minimum, and it can be assumed that the coupling between the warp and roll, pitch or lift is small enough to be neglected. Since the coupling can be neglected, the controller can be designed without considering the existing control loops for the comfort controller.

The block diagram of the transfer function from warp to yaw rate is shown in Figure 5.5 and the corresponding equation is:

$$G^*(s) = k_W G_{FCu1}(s) G_{uYr1}(s) - k_W G_{FCu2}(s) G_{uYr2}(s) - G_{FCu3}(s) \cdot \\ \cdot G_{uYr3}(s) + G_{FCu4}(s) G_{uYr4}(s) \tag{5.5}$$

In previous chapter it was mentioned that the response in yaw rate from a step in warp as input, initially goes in the wrong direction, due to the influence roll on an axle has on the steering angle. This means that there is a zero located in the right complex half plane leading to a non-minimum phase problem. However, this zero is very fast, meaning that it is located far into the right half plane and can therefore be neglected in the design of the controller. The bode plot of the plant[2] without taking into consideration the non-minimum phase effect, is shown in Figure 5.6.

[2]Driving straight ahead at 80 km/h and with a 0.4 degrees toe in front and 1.0 degrees rear.

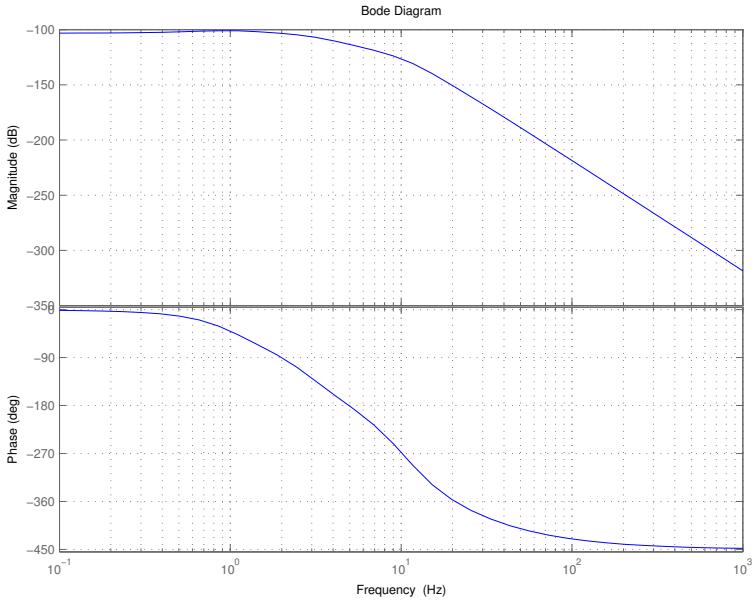

Figure 5.6 Warp to yaw rate transfer function

5.4 Design of PID controller

The design of the PID controller was carried out in Matlab SISO toolbox. The standard form of a PID controller in frequency domain, can be rewritten into rational form in which the design is done. The design of a PID controller is equal to placing a complex zero pair, a pole and then adding an integrator and a gain.

$$\begin{aligned} C(s) &= K_c\left(1+\frac{1}{sT_i}+\frac{sT_d}{\frac{sT_d}{N}+1}\right) = \\ &= K_c\frac{s^2\left(\frac{T_iT_d}{N}+T_iT_d\right)+s\left(T_i+\frac{T_d}{N}\right)+1}{sT_i\left(s\frac{T_d}{N}+1\right)} = \\ &= K_c\frac{\frac{T_d}{N}+T_d}{\frac{T_d}{N}}\cdot\frac{s^2+s\frac{T_i+\frac{T_d}{N}}{T_i\left(\frac{T_d}{N}+T_d\right)}+\frac{1}{T_i\left(\frac{T_d}{N}+T_d\right)}}{s\left(s+\frac{N}{T_d}\right)} = \\ &= K\frac{(s-z)(s-\overline{z})}{s(s-p)} = K\frac{s^2-2\mathrm{Re}zs+z\overline{z}}{s(s-p)} \end{aligned} \tag{5.6}$$

The parameters of the PID controller can then be expressed in terms of the gain, the pole and the zeros used in Matlab SISO toolbox:

$$\frac{T_d}{N} = -\frac{1}{p} \tag{5.7}$$

$$T_i = \frac{1}{p}-\frac{2\mathrm{Re}z}{z\overline{z}} \tag{5.8}$$

$$T_d = \frac{1}{T_i}\frac{1}{z\overline{z}}+\frac{1}{p} \tag{5.9}$$

$$K_c = K\frac{1}{1-T_dp} \tag{5.10}$$

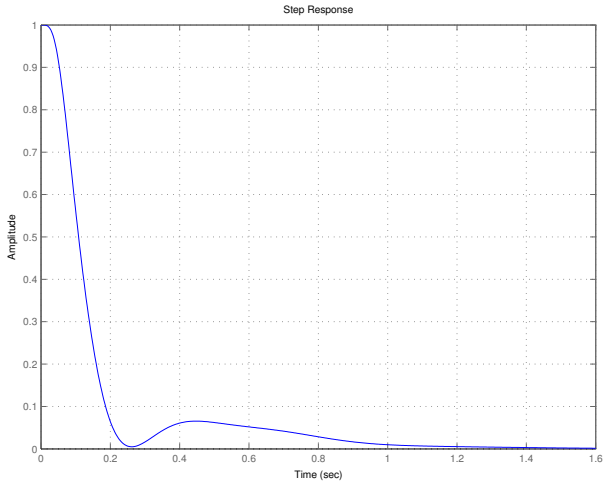

Figure 5.7 Step rejection of disturbance.

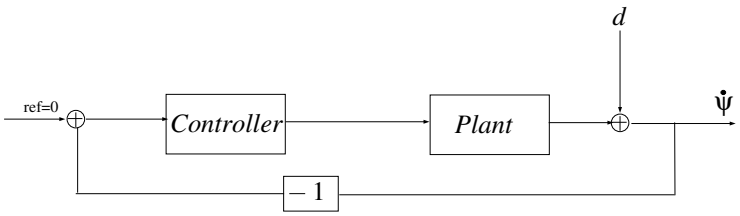

Figure 5.8 Standard feedback control loop.

The design was carried out by tuning the gain and placing the zeros and the pole until a satisfactory disturbance rejection was attained (see Figure 5.7). The open loop bode diagram is shown in Figure 5.9.

The PID controller was discretised (according to [1]) and implemented in CASCaDE. Because of the constraints on the actuators, i.e. saturating limits on the suspension struts, using an integrator can result in windup of the controller. The front actuators have a saturation limit of approximately 43 mm and the rear actuators of about 63 mm. As mentioned in previous chapter, it is not possible to use the full limits of the actuators, because the other controllers need to be given space to work. Therefore an actuator model with reduced limits, (also used for anti-windup) was introduced, making certain that the limits aren't fully reached during a heavy wind gust. The limits corresponds to a front position of the piston of 35 mm and to a rear position of 50 mm. The anti-windup was implemented according to [1] and it will not be presented here.

The controller was designed for a velocity of 80 km/h. To maintain the same closed loop characteristics for all speeds, gain scheduling has to be implemented into the controller. This has not been carried out in this work.

5.5 Results and limitations of the controller

The PID controller that was designed in previous section was implemented into the more realistic CASCaDE. It turned out to be possible to achieve better results of side wind rejection by doing small adjustments of the PID parameters in the controller that was implemented in CASCaDE. The limits of the actuators aren't enough to fully compensate for large disturbances in yaw rate. When heavy wind

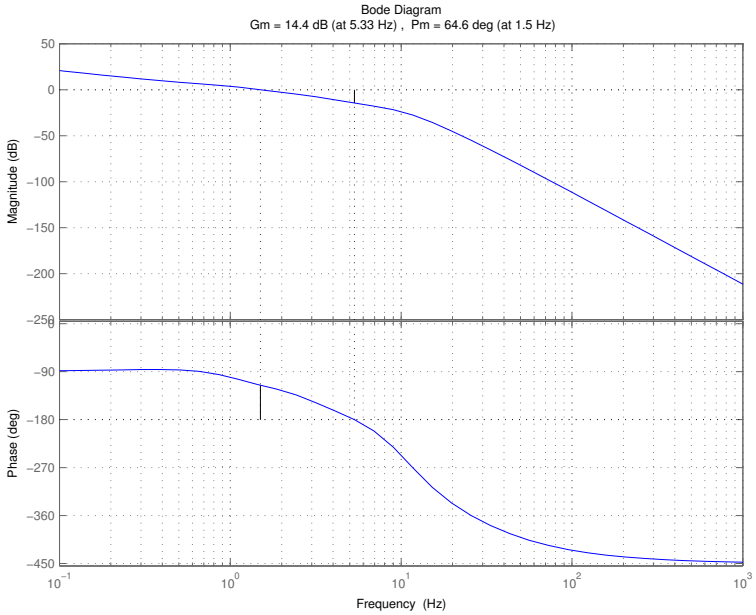

Figure 5.9 Bode plot of open loop.

gusts are acting on the vehicle, the saturation limits of the actuators are reached very fast, making the controller to be more of a *bang-bang control* character than a PID controller. Figure 5.10-5.13 shows the behavior of the vehicle with and without the controller driving at a speed of 80 km/h and exposing the vehicle to a wind gust of 20 m/s.

In Figure 5.10 it can be seen that there is a large overshoot when the wind disappears. This effect is due to the integral action of the controller. A PD controller was also evaluated leading to a smaller overshoot but then the yaw rate during wind couldn't be reduced to the same level as when using integral action. In Figure 5.12, it is illustrated how the side slip angle increases with control of the yaw rate and since it is not possible to control the side slip angle of the vehicle at the same time as the yaw rate with only one input, another input has to be used for control of the side slip angle.

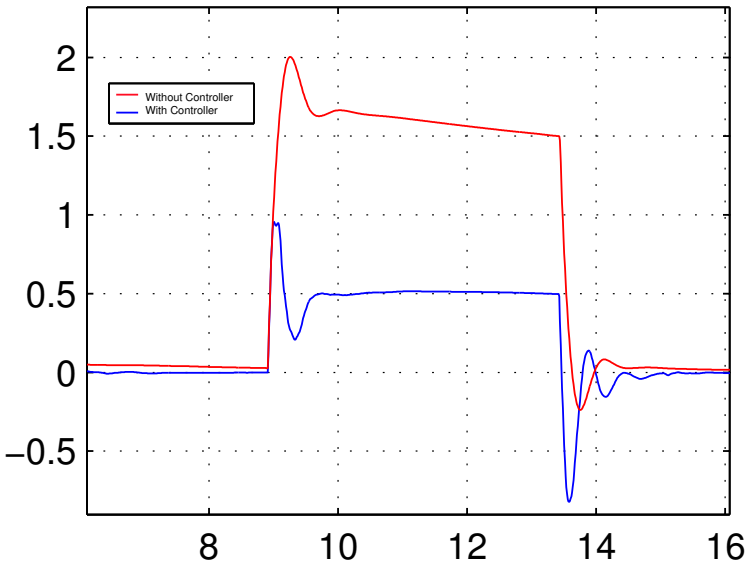

Figure 5.10 Yaw rate controlled and uncontrolled at a wind gust

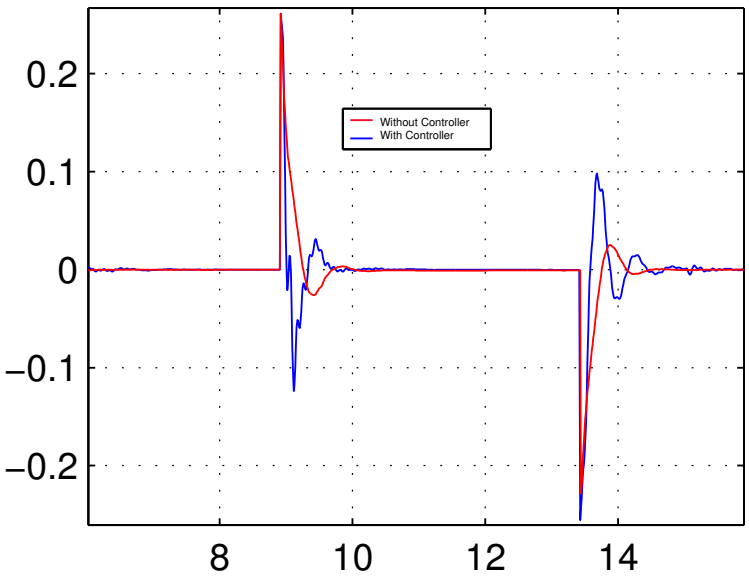

Figure 5.11 Yaw acceleration when the yaw rate is controlled and uncontrolled at a wind gust

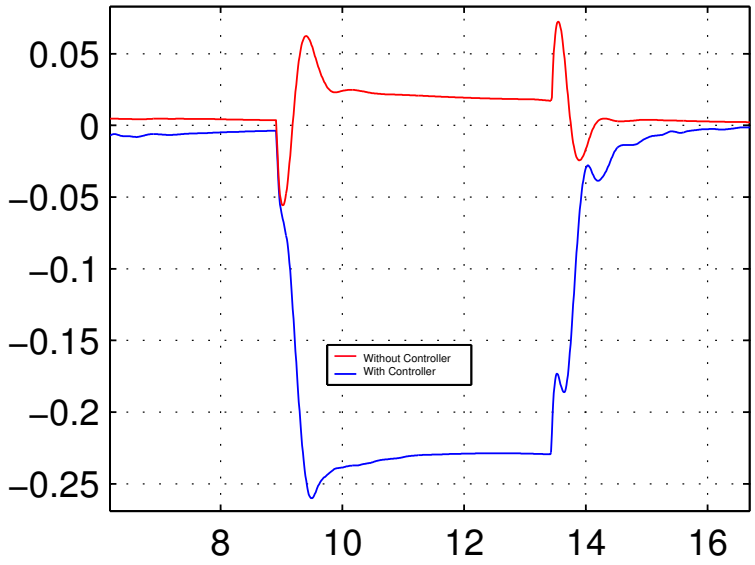

Figure 5.12 Side slip angle when the yaw rate is controlled and uncontrolled at a wind gust

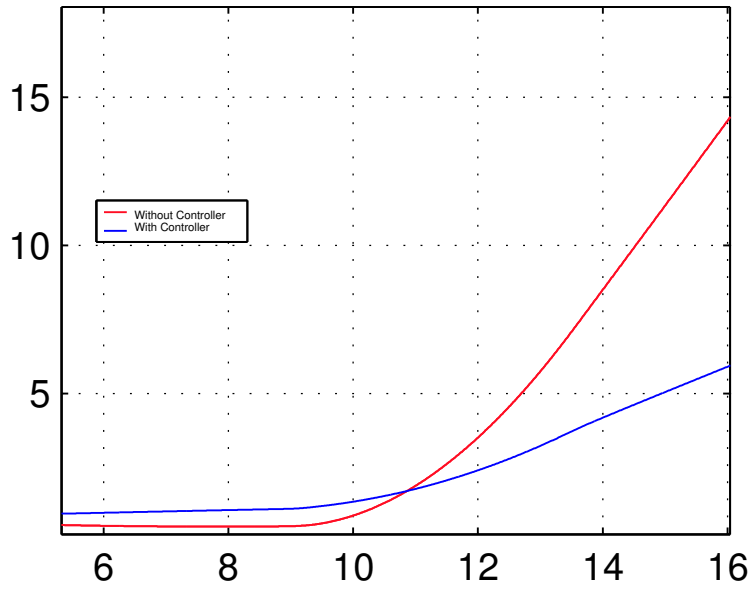

Figure 5.13 Position when the yaw rate is controlled and uncontrolled at a wind gust

6. Conclusions and future work

6.1 Conclusions

The main concept of this work has been to investigate how the interaction between lateral and vertical dynamics for a four-wheeled vehicle can be used for attenuating effects of wind gusts. How well the rejection of wind gusts turns out to be, mainly depends on how the toe in angles have been set on the vehicle. With greater toe in angles, greater side forces can be produced on the tyres, thus leading to a larger yaw moment when warp is applied. The toe in angles used in this work, i.e. 0.4 degrees front and 1.0 degrees rear, are greater than the toe in angles set on an ordinary model. By working with these values it is possible to reduce the effects wind gusts have on the yaw rate using feedback control with warp as input to the vehicle. But by controlling the yaw rate, the side slip angle is increased.

6.2 Future Work

The design of the controller was carried out under the assumption that the wind could be observed. Therefore an observer could be designed that extracts information on how the wind is influencing the dynamics of the vehicle. The simulations carried out in CASCaDE should also be verified with real tests on the Technoshuttle. The controller was designed for a velocity of 80 km/h and to maintain the same closed loop characteristics for all velocities gain scheduling has to be implemented.

Further, the PID controller causes a large overshoot when the wind disappears and it could be investigated how this overshoot can be reduced. In addition to this, it should be investigated what appropriate actions that needs to be taken against the increasing body side slip angle that can't be controlled with the same input. Since the toe in angles that have been used aren't the same ones as on the real vehicle, it could be motivated to construct a switch that sets the toe in angles on the rear wheels to a certain value, preferably as large as possible when wind is present.

7. Bibliography

[1] Karl J. Åström and Björn Wittenmark. *Computer Controlled Systems: Theory and Design*. Prentice Hall, 3 edition, 1997.

[2] Lars Nyborg Egbert Bakker and Hans B. Pacejka. Tyre modelling for use in vehicle dynamics studies. SAE Technical Paper Series 870421, Chassis Engineering Group Volvo Car Corp, Vehicle research Laboratory Delft University of Technology, 1987.

[3] Wolfgang Sienel Jürgen Ackermann, Tilman Bünte. Driving safety using robust steering control.

[4] J.L. Meriam and L.G. Kraige. *Engineering Mechanics DYNAMICS*. Wiley, 4:th edition, 1998. SI Version.

[5] N.Lazic. Optimal vehicle dynamics– yaw rate and side slip angle control using 4-wheel steering. Master's thesis, Department of Automatic Control, Lunds Universitet, Lund, Sweden, October 2002.

[6] Ralph H. Streiter. *Entwicklung und Realisierung eines analytischen Regelkonzeptes für eine aktive Federung*. Phd thesis, ISS-Fahrzeugtechnik, Technische Universität Berlin, Berlin, Germany, November 1996.

[7] Kai Wulff. Four-wheel steering vehicle- part 1:modeling. November 2000.

[8] Z.Zomotor. Bestimmung des schwimmwinkels mit regelungstechnischen methoden. Master's thesis, Institut für Regelungstechnik, Universität Stuttgart, Stuttgart, Germany, 1992.

Notation

Variables and parameters

v_x	The forward velocity, in the direction of x_{CG}
v_y	The lateral velocity, in the direction of y_{CG}
$\dot{\psi}$	Yaw rate (rotation about z_{CG})
δ_i	Wheel steering angle
v	The resulting velocity
β	Vehicle body side slip angle (angle between x_{CG} and v_{CG}, the vehicle velocity)
F_{yi}	Lateral wheel ground contact force (acting in the direction of y_{Wi})
F_{xi}	Longitudinal wheel ground contact force (acting in the direction of x_{Wi})
γ_i	Geometry parameter
h_i	Geometry parameter
θ_1	Geometry parameter
f_{xi}, f_{yi}	tyres forces in body-fixed coordinates
a_x, a_y	Longitudinal and lateral acceleration
m_i	Torque caused by single wheel
$\ddot{\psi}$	Yaw angular acceleration
I_{zz}	Moment of inertia about vertical axis
x_B, y_B, z_B	Axis for the center of gravity coordinate system
l_f, l_{r^*}	The x-component of the distance from CG to suspension systems front and rear
l_l, l_r	The y-component of the distance from CG to suspension system
l_{L_i}	The y-component of the distance from CG to bearing mount
l_{W_i}	The y-component of the distance from CG to wheel
l_{ss_i}	The y-component of the distance from CG to suspension strut
$l_{fr}, l_{fl}, l_{rr}, l_{rl}$	The indices stands for Front Right .. Rear Left

z_{PP}, z_{RP}	The vertical distance from ground level to the pitch- and roll axis respectively
z_{B0}	The vertical distance from ground level to CG
z_L	The vertical distance from ground level to bearing mount
z_{ssB}	The vertical distance from ground level to upper suspension mounting point
z_{ssL}	The vertical distance from ground level to lower suspension mounting point
r, p	Roll- and pitch angle respectively
M_r, M_p	Roll- and pitch moment respectively
J_x, J_y	Roll- and pitch moment of inertia respectively
F_z	Disturbance force in vertical direction
m_B, m_W	Body- and wheel mass respectively
$\underline{F}_{ss}$	Forces in suspension strut
$\underline{F}_L$	Forces in bearing mount
c_{Bf}, c_{Br}	Suspension spring constants front and rear
b_{Bf}, b_{Br}	Suspension damper constants front and rear
u_{ij}	Suspension system control signal
c_W	Tyre spring constant
w_{ij}	Road profile at tyre contact "point"
F_{i_B}	Force acting on upper suspension mounting point
J_r, J_p	Moment of inertia of body about roll and pitch axis respectively
T_{G_i}	Geometry matrices for vertical model
H	Matrix containing road to suspension forces transmission ratios
A_1, A_2	Matrices containing spring and damper constants
λ_i	Slip of the wheel
ω_i	Angular velocity of wheel
v_{Wi}	Absolute velocity of wheel
α_i	Tyre side slip angle
r_{Wi}	Dynamical radius of wheel
ξ_i	Normalised wheel slip
C_i^*	Normalised stiffness
μ_i	Friction coefficient
F_Z	Wheel load
n_L	Caster coefficient

J	Moment of inertia for steering system
b, c	Damping and spring coefficients for steering system
β	Aerodynamic stream angle
ρ	Density of air
c_F, c_M	Shape factors
v	Absolute velocity of air flow
A	Reference surface
l	Distance between front and rear wheels
T_a	Actuator time constant
K_a	Actuator gain
$\underline{i}$	Currents to actuators.
Ω	Warp
$G_{uRi}(s)$	Transfer function from position of piston to roll angle
$G_{FCui}(s)$	Transfer function from Force controller input to position of piston.
$F_{FCi}(s)$	Reference value to force controller
k_W	Weighting factor
Ω^*	The input signal warp
$G^*(s)$	Transfer function from warp to yaw rate
$G_{uYr1}(s)$	Transfer function from piston position to yaw rate
$C(s)$	Controller Transfer function
K_c, T_i, T_d, N	PID parameters

Appendix A.

A.1 Sensor signals

Below follows the derivation of how sensor signals can be constructed with center of gravity values. These signals were derived for comparison to sensor signals in CASCaDE. There are five sensors in the vehicle that were compared. Three are pointing in the vertical direction of the body and they don't consider the gravitational constant. The other two are pointing in the lateral and the vertical directions of the body respectively and they consider the gravitational constant. Equation A.1 computes the accelerations in the position of a specific sensor in the global coordinate system (see [4]).

$$\mathbf{a}_{SP} = \mathbf{a}_{CG} + \dot{\boldsymbol{\omega}} \times \mathbf{r} + \boldsymbol{\omega} \times (\boldsymbol{\omega} \times \mathbf{r}) + 2\boldsymbol{\omega} \times \mathbf{v}_{rel} + \mathbf{a}_{rel} \tag{A.1}$$

In the equation above, $\mathbf{r}$ is the vector containing the distances to the position of the sensor, $\boldsymbol{\omega}$ is the vector containing the angular velocities. Since the chassis is modelled as infinitely stiff there is no relative motion between the center of gravity and the sensor positions. This means that the two last terms are not considered. For the sensors with gravitation considered, the constant of gravitation is added in the vertical direction.

To transform the three accelerations in a given sensor point corresponding to the signal of the sensor (which is positioned in the moving coordinate system), the direction of the sensor needs to be known as well as the angles of the chassis, i.e. the roll and pitch angles. The accelerations in equation A.1 are computed so that the directions are the same as in the global coordinate system and not the same as in the body fixed coordinate system. This means that a transformation from the body directions to the global directions needs to be carried out. Below follows how the transformation was carried out by considering the roll and pitch angles of the body.

$$\mathbf{D}_{RotX} = \begin{pmatrix} 1 & 0 & 0 \\ 0 & \cos(r) & -\sin(r) \\ 0 & \sin(r) & \cos(r) \end{pmatrix} \tag{A.2}$$

$$\mathbf{D}_{RotY} = \begin{pmatrix} \cos(p) & 0 & \sin(p) \\ 0 & 1 & 0 \\ -\sin(p) & 0 & \cos(p) \end{pmatrix} \tag{A.3}$$

The full transformation, $\mathbf{D}_{RotYX}$ is attained by multiplying $\mathbf{D}_{RotY}$ with $\mathbf{D}_{RotX}$ and we arrive at:

$$\overline{\mathbf{n}} = \underbrace{\begin{pmatrix} \cos(p) & \sin(p)\sin(r) & \sin(p)\cos(r) \\ 0 & \cos(r) & -\sin(r) \\ -\sin(p) & \cos(p)\sin(r) & \cos(p)\cos(r) \end{pmatrix}}_{\mathbf{D_{RotYX}}} \overline{\mathbf{n}}'' \tag{A.4}$$

If the direction of a specific sensor in the body coordinate system is given by the vector $\overline{\mathbf{n}}'' = (n_x'', n_y'', n_z'')^T$, the sensor signal is attained by projecting the accelerations computed in A.1, on the vector that contains the direction of the sensor in the global coordinate system, i.e. $\overline{\mathbf{n}} = \mathbf{D_{RotYX}}\overline{\mathbf{n}}''$. This leads to equation A.5.

$$a_{SS} = (\mathbf{D}_{RotYX}\overline{\mathbf{n}}^{''})^T \mathbf{a}_{SP} \tag{A.5}$$

For the longitudinal ($\overline{\mathbf{n}}^{''}_{xdir} = (1,0,0)^T$), lateral ($\overline{\mathbf{n}}^{''}_{ydir} = (0,1,0)^T$) and vertical ($\overline{\mathbf{n}}^{''}_{zdir} = (0,0,1)^T$) sensors the following equations are attained.

$$a_{SS_x} = \begin{pmatrix} \cos(p) & \sin(r)\sin(p) & \cos(r)\sin(p) \end{pmatrix} \begin{pmatrix} a_{SP_x} & a_{SP_y} & a_{SP_z} \end{pmatrix}^T \tag{A.6}$$

$$a_{SS_y} = \begin{pmatrix} 0 & \cos(r) & -\sin(r) \end{pmatrix} \begin{pmatrix} a_{SP_x} & a_{SP_y} & a_{SP_z} \end{pmatrix}^T \tag{A.7}$$

$$a_{SS_z} = \begin{pmatrix} -\sin(p) & \sin(r)\cos(p) & \cos(r)\cos(p) \end{pmatrix} \begin{pmatrix} a_{SP_x} & a_{SP_y} & a_{SP_z} \end{pmatrix}^T \tag{A.8}$$

A.2 Simulink Model

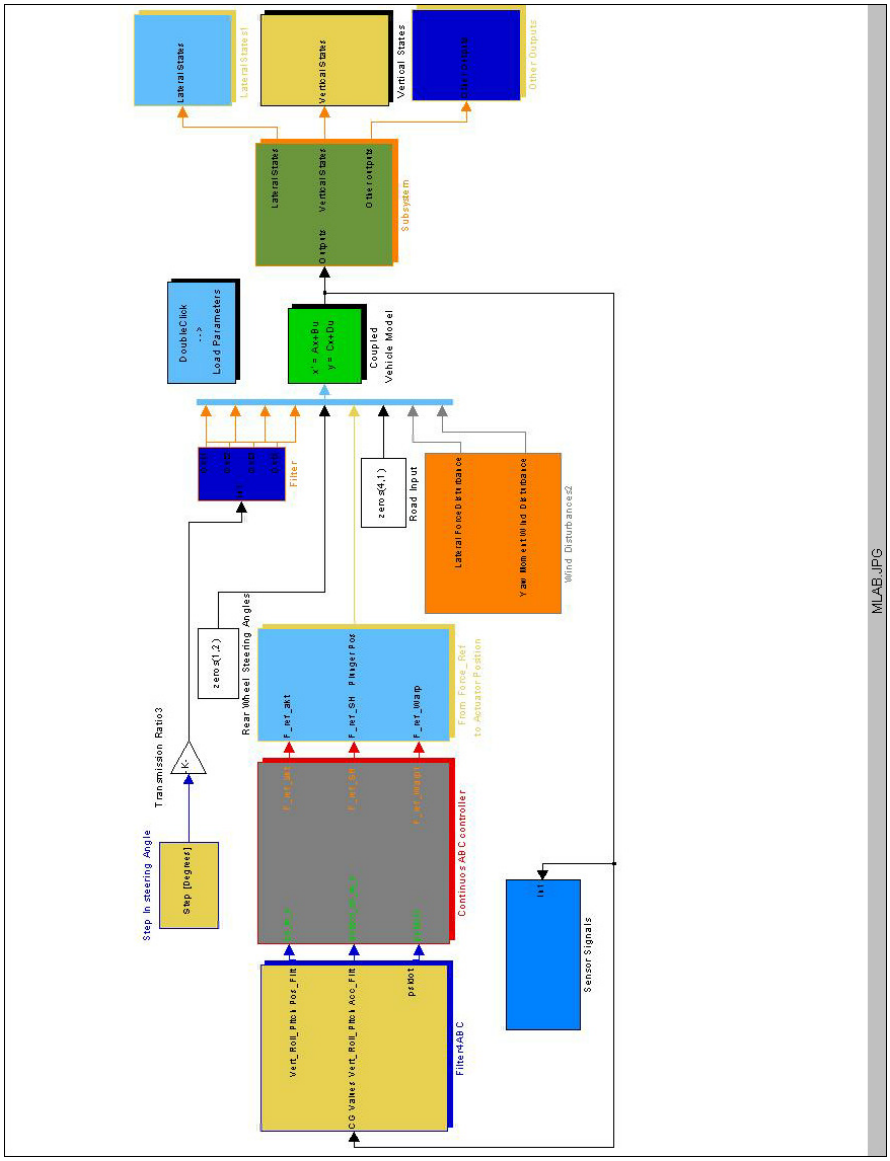

A.3 Main Matlab file

The file below is the main file that builds up the matrices for the state space representation and it also calls other sub-files but these aren't included here.

```
clear all;
%Car Mass
m=2364;
%Moment of Inertia about z-axis
J=4488; %Moment of Inertia around z-axis
%Initial conditions
Vx0=80/3.6; Vy0=0; psidot=0;
%-----------------Steering angle -------------------------
toe_In=zeros(4); toe_In(1,1)=0.5*pi/180;
toe_In(2,1)=-0.5*pi/180;
toe_In(3,1)=1.0*pi/180; toe_In(4,1)=-1.0*pi/180;

delta=zeros(4,1);% Determine point which about
                 %the car is to be linearized
delta(1,1)=0; delta(2,1)=0; delta(3,1)=0; delta(4,1)=0;

delta(1,1)=delta(1,1)+toe_In(1,1);
delta(2,1)=delta(2,1)+toe_In(2,1);
delta(3,1)=delta(3,1)+toe_In(3,1);
delta(4,1)=delta(4,1)+toe_In(4,1);

%Settings for Tires
FzN=8000; rdyn=0.328; Angvel=zeros(4,1);
Angvel(1:2,1)=Vx0/rdyn;
Angvel(3:4,1)=Vx0/rdyn;

muh=ones(4,1);% Friction Coefficients

%Car Geometry

LV=1.67; LH=1.41; SPBL=0.787; SPBR=0.787;

length=zeros(4,1); length(1,1)=sqrt(SPBR*SPBR+LV*LV);
length(2,1)=sqrt(SPBL*SPBL+LV*LV);
length(3,1)=sqrt(SPBR*SPBR+LH*LH);
length(4,1)=sqrt(SPBL*SPBL+LH*LH);

teta=zeros(4,1); teta(1,1)=-atan(SPBR/LV);
teta(2,1)=atan(SPBL/LV); teta(3,1)=pi+atan(SPBR/LH);
teta(4,1)=pi-atan(SPBL/LH);

% Static vertical forces on Vehicle. Moment equation about
% the Tires.

Fz=zeros(4,1); Fz(1,1)=5308; Fz(2,1)=5308; Fz(3,1)=6287;
Fz(4,1)=6287;


%------Compute Angular Velocity to achieve Fx_CoG=0----
Angvel=CompensateLongitudinalForce(Vx0,Vy0,psidot,teta,...
        .....length,Angvel,delta,Fz,FzN,muh);
% Computing derivatives of the dynamic tyre model
```

```
EinlaufDer=ComputeEinlaufDerivatives(Vx0,Vy0,psidot,teta,..
        .......length,Angvel,delta,Fz,FzN,muh);

%-----------------------------A-MATRIX---------------------
A=zeros(7); forward=1e-6; Fy=zeros(4,1); Fx_CoG=0; Fy_CoG=0;

for i=1:4
  [Fx,Fy(i,1)]=ComputeTireForces(Vx0,Vy0,psidot,...
     ...teta(i,1),length(i,1),Angvel(i,1),delta(i,1),....
     ....Fz(i,1),FzN,muh(i,1));
  Fx_CoG=Fx_CoG-Fy(i,1)*sin(delta(i,1))+Fx*cos(delta(i,1));
  Fy_CoG=Fy_CoG+Fy(i,1)*cos(delta(i,1))+Fx*sin(delta(i,1));
end;

%------------Row 1 in A- Matrix------------
pointTerm1=Computef1(Vx0,Vy0,psidot,teta,length,Angvel,...
            ...delta,Fz,FzN,Fy,m,muh);

df1_dVy=(Computef1(Vx0,Vy0+forward,psidot,teta,length,...
    ....Angvel,delta,Fz,FzN,Fy,m,muh)-pointTerm1)/forward;
df1_dpsidot=(Computef1(Vx0,Vy0,psidot+forward,teta,length,.
      ...Angvel,delta,Fz,FzN,Fy,m,muh)-pointTerm1)/forward;



for i=1:4
    Fy(i,1)=Fy(i,1)+forward;
    df1_dFyi=(Computef1(Vx0,Vy0,psidot,teta,length,Angvel,.
        .......delta,Fz,FzN,Fy,m,muh)-pointTerm1)/forward;
    A(1,i+3)=df1_dFyi;
    Fy(i,1)=Fy(i,1)-forward;
end;


A(1,1)=df1_dVy; A(1,3)=df1_dpsidot;


%------------Row 2 in A- Matrix------------

A(2,3)=1;

%------------Row 3 in A- Matrix------------

pointTerm2=Computef3(Vx0,Vy0,psidot,teta,length,Angvel,...
        ...delta,Fz,FzN,Fy,J,muh);
df3_dVy=(Computef3(Vx0,Vy0+forward,psidot,teta,length,.....
      ...Angvel,delta,Fz,FzN,Fy,J,muh)-pointTerm2)/forward;
df3_dpsidot=(Computef3(Vx0,Vy0,psidot+forward,teta,length,.
   ......Angvel,delta,Fz,FzN,Fy,J,muh)-pointTerm2)/forward;

A(3,1)=df3_dVy; A(3,3)=df3_dpsidot;

for i=1:4
    Fy(i,1)=Fy(i,1)+forward;
    df3_dFyi=(Computef3(Vx0,Vy0,psidot,teta,length,Angvel,.
        ...delta,Fz,FzN,Fy,J,muh)-pointTerm2)/forward;
    A(3,i+3)=df3_dFyi;
```

```
    Fy(i,1)=Fy(i,1)-forward;
end;

%-------------Row 4-7 in A-Matrix-------------
for i=1:4
     A(i+3,1)=EinlaufDer(i,2);
     A(i+3,3)=EinlaufDer(i,3);
     A(i+3,i+3)=EinlaufDer(i,4);
end;

%-----------------------------B-MATRIX--------------------
B=zeros(7,8); % Eight input signals. Four Tire angles and
              % four Wheel Loads

pointTerm1=Computef1(Vx0,Vy0,psidot,teta,length,Angvel,....
        ....delta,Fz,FzN,Fy,m,muh);
for i=1:4
    delta(i,1)=delta(i,1)+forward;
    df1_dDelta=(Computef1(Vx0,Vy0,psidot,teta,length,....
    .....Angvel,delta,Fz,FzN,Fy,m,muh)-pointTerm1)/forward;
    B(1,i)=df1_dDelta;
    delta(i,1)=delta(i,1)-forward;
end;

pointTerm1=Computef1(Vx0,Vy0,psidot,teta,length,Angvel,...
        ...delta,Fz,FzN,Fy,m,muh);
for i=1:4
    Fz(i,1)=Fz(i,1)+forward;
    df1_dFz=(Computef1(Vx0,Vy0,psidot,teta,length,Angvel,..
        ......delta,Fz,FzN,Fy,m,muh)-pointTerm1)/forward;
    B(1,i+4)=df1_dFz;
    Fz(i,1)=Fz(i,1)-forward;
end;

pointTerm2=Computef3(Vx0,Vy0,psidot,teta,length,....
            .....Angvel,delta,Fz,FzN,Fy,J,muh);
for i=1:4
    delta(i,1)=delta(i,1)+forward;
    df3_dDelta=(Computef3(Vx0,Vy0,psidot,teta,length,...
    ....Angvel,delta,Fz,FzN,Fy,J,muh)-pointTerm2)/forward;
    B(3,i)=df3_dDelta;
    delta(i,1)=delta(i,1)-forward;
end;

pointTerm2=Computef3(Vx0,Vy0,psidot,teta,length,Angvel,...
    ...delta,Fz,FzN,Fy,J,muh);
for i=1:4
    Fz(i,1)=Fz(i,1)+forward;
    df3_dFz=(Computef3(Vx0,Vy0,psidot,teta,length,Angvel,..
         .......delta,Fz,FzN,Fy,J,muh)-pointTerm2)/forward;
    B(3,i+4)=df3_dFz;
    Fz(i,1)=Fz(i,1)-forward;
end;

for i=1:4
    B(i+3,i)=EinlaufDer(i,1);
    B(i+3,i+4)=EinlaufDer(i,5);
```

```
end;

C=eye(7); D=zeros(7,8);

VerticalModel;% Calling the model for the vertical dynamics


%-------Distance Roll Axis to CoG-----------

dist1=-0.2; % Roll axis 0.2 m below ground level
hCoG=0.286; rstat=0.308;

CoG_Rollaxis=rstat+hCoG-dist1;

%-------------------------------------------

A21State=zeros(21); B21State=zeros(21,14);

%---------------------New A-Matrix---------------
% Values from Lateral equations
A21State(1:7,1:7)=A; A21State(1:7,11:14)=-cR*B(1:7,5:8);

% Values from Vertical equations
A21State(8:21,8:21)=Asim;

% Mx is no longer considered an input signal but rather a
        % combination of states
A21State(17,3)=Vx0/Jw*mA*CoG_Rollaxis;

for i=1:7
    A21State(17,i)=1/Jw*mA*CoG_Rollaxis*A(1,i)+...
    ...+A21State(17,i);
end;

for i=1:4
    A21State(17,i+10)=A21State(17,i+10)-cR*B(1,i+4)*1/....
    .../Jw*mA*CoG_Rollaxis;
end;

%------------------------------------------------------------
%---------------------New B-Matrix------------------------
% Values from Lateral equations
B21State(1:7,1:4)=B(:,1:4);% Equations for the angle of the
                           % wheel
B21State(1:7,11:14)=cR*B(1:7,5:8);

% Values from Vertical equations
Btemp=Bsim; clear Bsim; Bsim=[Btemp(:,1:6) Btemp(:,8:11)];

B21State(8:21,5:14)=Bsim;

for i=1:4
    B21State(17,i)=B21State(17,i)+B(1,i)/Jw*mA*CoG_Rollaxis;
    B21State(17,i+10)=B21State(17,i+10)+B(1,i+4)*cR/Jw*mA*..
            ...*CoG_Rollaxis;
end;
```

```
%------------Building up new State Space model where------
%-------------steering system dynamics are included.------
%------------Arrive at a 25 states State space Model.-----
%--------The first 4 states are the dynamics describing---
%-----------------the steering system---------------------


A25State=zeros(25); B25State=zeros(25);

% The new states, i.e. the angle and the angular velocities
% about the z-axis for the front wheels are introduced as
% the first 4 states of the expanded state space model
% Steerangle at wheels were previously inputs but when
% introducing dynamics for the steering system
% the earlier sensitivities with respect to the inputs are
% now instead sensitivities with respect to the states x1
% and x3, i.e. the two steerangles at the wheels.

A25State(5:25,5:25)=A21State;
A25State(5:25,1)=B21State(:,1);
A25State(5:25,3)=B21State(:,2);

B21State(:,1)=zeros(21,1); B21State(:,2)=zeros(21,1);

% When including the dynamics of the steering system
% the input vector increases in size since the  derivative
% of the steering angle is now also used as input, i.e. two
% extra inputs!

B25State=[zeros(4,16);zeros(21,2) B21State];

InvSteerStiff=1/210000; NaturalFreq=sqrt(100); Damping=0.9;

A25State(1,2)=1; A25State(2,1)=-NaturalFreq*NaturalFreq;
A25State(2,2)=-2*NaturalFreq*Damping;
A25State(2,8)=-InvSteerStiff*NaturalFreq*NaturalFreq;

B25State(2,1)=NaturalFreq*NaturalFreq;
B25State(2,2)=2*NaturalFreq*Damping;

A25State(3,4)=1; A25State(4,3)=-NaturalFreq*NaturalFreq;
A25State(4,4)=-2*NaturalFreq*Damping;
A25State(4,9)=-InvSteerStiff*NaturalFreq*NaturalFreq;

B25State(4,3)=NaturalFreq*NaturalFreq;
B25State(4,4)=2*NaturalFreq*Damping;



%==========================================================
%==========================================================
%                Model including the disturbances
%                caused by the wind
%==========================================================
%==========================================================
```

```
A_Fini=A25State;

B_Fini=
   =[B25State(1:25,1:10) B25State(1:25,13:16) zeros(25,2)];
B_Fini(7,15)=1/m; B_Fini(9,16)=1/J;

C_Fini=zeros(34,25); C_Fini(1:25,1:25)=eye(25);

D_Fini=zeros(34,16);

for i=1:4           % Wheel loads
    C_Fini(26+i,14+i)=-cW;
    D_Fini(26+i,10+i)=cW;
end;

%Outputs: Lateral Acceleration, wheel loads, Vertical
% acceleration, etc

% Lateral Acceleration
C_Fini(26,:)=A_Fini(5,:); C_Fini(26,7)=C_Fini(26,7)+Vx0;
D_Fini(26,:)=B_Fini(5,:);

%Vertical Acceleration
C_Fini(31,:)=A_Fini(19,:); D_Fini(31,:)=B_Fini(19,:);

%Pitch Acceleration
C_Fini(32,:)=A_Fini(20,:); D_Fini(32,:)=B_Fini(20,:);

%Roll Acceleration
C_Fini(33,:)=A_Fini(21,:); D_Fini(33,:)=B_Fini(21,:);

%Yaw Acceleration
C_Fini(34,:)=A_Fini(7,:); D_Fini(34,:)=B_Fini(7,:);


% Fz is Moved to the new input vector! Dist_Vec=[F_y M_z]
SideWindSpeed=72/3.6;
[Fx_Wind,Fy_Wind,Fz_Wind,Mx_Wind,My_Wind,Mz_Wind]=
        =Windmodel(Vx0,SideWindSpeed);
sensor_lengths;
```